Biointerface Research in Applied Chemistry
Open-Access Journal (ISSN: 2069-5837)

Article
Volume 14, Issue 2, 2024, 36
https://doi.org/10.33263/BRIAC142.036

Synthesis, Spectral Characterization of Novel Isatin Schiff Base Metal Complexes: Biological Activities Evaluation and Molecular Docking Studies

Neelufar [1], Syed Hidayathulla [2], Javarappa Rangaswamy [3], Nagaraja Naik [1,*]

[1] Department of Studies in Chemistry, University of Mysore, Manasagangotri, Mysuru–570006, Karnataka, India; neelufar.syeda@gmail.com (N.);
[2] Department of Molecular biology, University of Mysore, Manasagangotri, Mysuru–570006, Karnataka, India; hidayathsyed@gmail.com (S.H.);
[3] Department of Chemistry, Poornaprajna College, Shri Admar Mutt Education Council, Mangalore University, Udupi, Karnataka, India.; rangaswamyteertha@gmail.com (J.R.);
* Correspondence: drnaikchem@gmail.com (N.N.);

Scopus Author ID: 57225381566
Received: 13.02.2023; Accepted: 24.06.2023; Published: 4.02.2024

Abstract: A new series of novel isatin Schiff base metal complexes have been synthesized. The structure of the synthesized ligand and metal complexes is characterized by 1H-NMR, 13C-NMR, LC-MS, UV-Vis, FTIR, SEM, EPR, TGA, and Elemental analysis. Based on the characterization, it was revealed that the Schiff base ligand existed as a bidentate ligand, Cu(II) complex (6b) showed distorted square planar geometry, and the remaining complexes (6a, 6c-h) were octahedral geometry. Molar conductivity data showed that all the metal complexes are electrolytic. Further, the ligand (L6) and its metal complexes were screened for their in vitro antidiabetic, anticancer, and DNA cleavage activities. Among the synthesized complexes, Co(II) metal complex (6e) exhibited the highest antidiabetic and anticancer activity against HepG2 (Liver) and MDA-MB 231 (Breast) cancer cells. The ligand and complexes were found to cleave the pBR322 plasmid DNA during gel electrophoresis studies. The molecular docking with 5NN5, 4GQR, and 3KJF mutant protein was done for the optimization of the investigated complex as potential amylase, glucosidase, and cancer cell inhibitors, and obtained docking score was in very good agreement with experimental data.

Keywords: isatin Schiff base; metal complexes; anti-microbial activity; antioxidant; DNA cleavage.

1. Introduction

Isatin is a flexible chemical building block containing an indole ring, commonly known as 1H-indole-2, 3-dione. Isatin derivatives have a variety of biological actions, including antiviral, antibacterial, antifungal, anticonvulsant, anti-tubercular, anti-microbial, and anticancer effects [1]. Isatin, an endogenous natural compound derived from several plants, is used as a common scaffold in a variety of drugs, agrochemicals, and colors [2]. Derivatives of isatin, such as substituted isatins, hydrazones, Mannich bases, Schiff bases, and spiroindolinones, exhibit a variety of biological activities [3]. Among the isatin derivatives, oxindole is a versatile precursor that may be used to make a variety of heterocyclic compounds, including many synthetic medicines [4], and it is acknowledged as a natural product [5]. Other isatin derivatives, such as semaxanib and SU-11248 have anti-angiogenic and tyrosine kinase inhibitory properties [6].

Moreover, isatin was chosen as a biologically active frame for coupling because it is thought to be a sophisticated spectrum of heterocyclic moieties with various pleasing activities and superior acceptance in humans [7]. The major proteinase of SARS-CoV-1 and SARS-CoV-2, 3C-like protease (3CLpro), has also been reported to be inhibited by isatin derivatives [8]. The multicomponent reaction based on isatin is used to develop bioactive and druglike compounds [9, 10]. Isatin belongs to a significant class of aromatic heterocyclic chemicals present in both plant and human tissue and also has various biological uses, including antileishmanial and anticonvulsant properties [11-14]. In addition to this, the literature describes the Schiff bases of isatin metal complexes and reveals a wide spectrum of antipathogenic capabilities, including antiviral, anti-mycobacterial, anti-tubercular, and antifungal effects [15]. Many pharmaceutical products available on the market today use the active scaffold 1H-indole-2,3-dione, such as indirubin and methisazone [16, 17]. Earlier, we had reported on synthesizing Schiff base metal complexes and evaluating their biological activities [18-20]. The present study deals with the synthesis of novel isatin Schiff base and its Cu(II), Ni(II), Co(II), and Ru(III) complexes and evaluates their biological activities along with molecular docking studies.

2. Materials and Methods

All chemicals used in this study were of purest grade, purchased from Sigma Aldrich, and used without further purification. The chemical composition of various elements (C, H, O, N) and their extent of distribution of imine base ligand and their metal complexes were analyzed by using Perkin Elmer 240°C elemental analyzer. Mass spectra were recorded using LC-MS/MS Synapt G2 HDMS. FTIR Spectra of the Schiff base and their corresponding metal complexes were recorded in the range of 4000-400 cm^{-1} in Shimadzu, japan, with KBr pellets. Electronic absorption spectra were recorded on a DU-730 UV Spectrometer in the 200-800 nm wavelength range using DMSO as a solvent. The magnetic susceptibility is measured at room temperature using Guoy balance with $Hg[Co(CN)_4]$ as a standard compound. The Proton ^1H NMR and Carbon ^{13}C NMR spectra of Schiff base were recorded in DMSO-d6 solvent using VNMR-400 Agilent NMR spectrometer with an operating frequency 400 MHz for ^1H NMR and 100MHz for ^{13}C NMR at an ambient temperature using trimethylsilane (TMS) as an internal reference. The molar conductance of metal complexes was measured on an Elico CM-180 conductivity meter with a cell constant of 1 cm^{-1}. The thermogravimetric (TGA) analysis was recorded on a ZSCH STA 2500 in the 25-900°C temperature range at a heating rate of 10 °C min^{-1} under a nitrogen atmosphere. Electron paramagnetic resonance (EPR) spectra were recorded using a JEOL JES-TE100 EPR spectrometer in DMSO solution at LNT in the solid state on X-band at a frequency of 9.13 GHz under the magnetic field of 300 mT. Powder XRD was recorded on a powder X-ray diffractometer smartlab3Kw. The morphology and particle size were recorded on a Zeiss Scanning Electron Microscope (SEM). The compounds' melting point was determined on a Thomas Hoover capillary melting point apparatus with a digital thermometer.

2.1. Chemical synthesis.

2.1.1 Synthesis of (Z)-2-((4-bromophenyl)imino)-5-fluoroindolin-3-one (L6).

The Schiff base ligand was synthesized by reacting an equimolar reaction of 5-flouroisatin and 4-bromoaniline and a few drops of Glacial acetic acid in ethanol. The reaction

mixture was refluxed for 5h with continuous stirring. The reaction was monitored by TLC using 9:1 (Hexane: Ethyl acetate). After 5h, the product obtained was filtered, washed with ethanol, recrystallized from ethanol, and dried under vacuum. **(**Scheme 1**)**

Yield: 87% Colour: Orange M.P: 262 °C Elemental analysis Calc. (found) (%);C: 52.69 (51.98) H: 2.53 (2.18) N: 8.78 (8.14); ^{1}H NMR (400MHz) (DMSO-d_6): 10.43 (s, 1H, NH), 7.17 (s,1H, CH=N), 5.36(d, 1H, OH), 4.81(d, 2H, CH_2), 6.86(dd, J=4.8Hz, 1H), 7.02(t, J=7.6Hz, 1H), 6.95 (1H), 6.92(d, J=7.6Hz, 1H), 7.16-7.13 (m) ^{13}C NMR: 62.7, 81.70, 111.36, 112.97, 113.2, 114.9, 117.69, 119..48,124.61, 127.64, 129.9, 130.0, 138.79, 140.4, 157.28, 159.65, 175.3ppm.

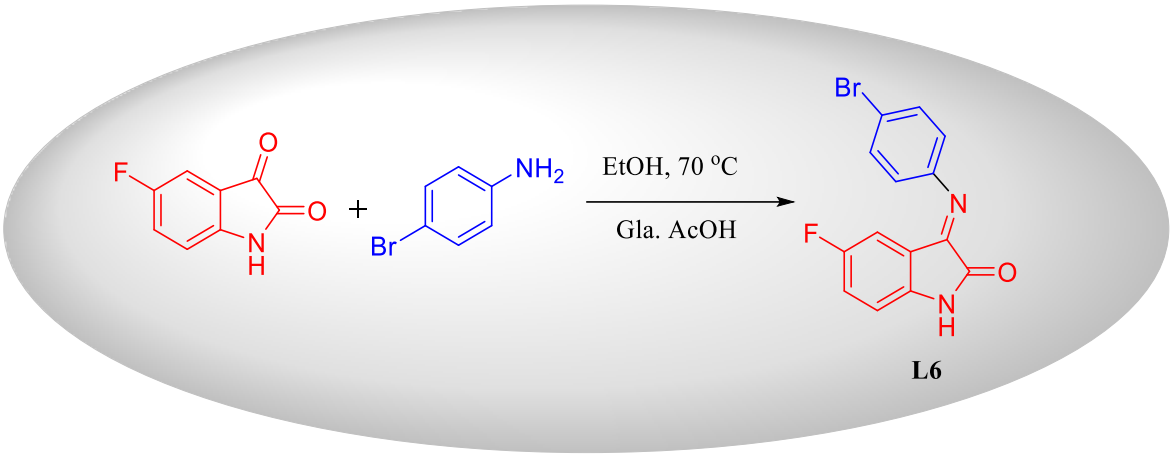

Scheme 1. Synthesis of (Z)-2-((4-bromophenyl)imino)-5-fluoroindolin-3-one (L6).

2.1.2. Synthesis of metal complexes.

The Schiff base ligand (2mmole) dissolved in hot ethanol (5mL) solution was added dropwise in an ethanolic (5mL) solution of corresponding metal salts (1mmole) and refluxed for 4-6 hrs at 70-75 °C. After completion of the reaction, a solid precipitate is formed and washed with cold ethanol followed by petroleum ether and dried in a vacuum under a desiccator over anhydrous $CaCl_2$.

2.1.3. Synthesis of mixed ligand metal complexes.

The ligand (L) (1mmole) dissolved in hot ethanol (5mL) solution was added dropwise in hot ethanol (5mL) solution of corresponding metal salts (1mmole), which was heated for 1 hour. The secondary ligand 1,10-phenanthroline was added and refluxed for 4-6 hrs at 70-75 °C. After completion of the reaction, a solid precipitate was formed, washed with cold ethanol, and dried (Scheme 2).

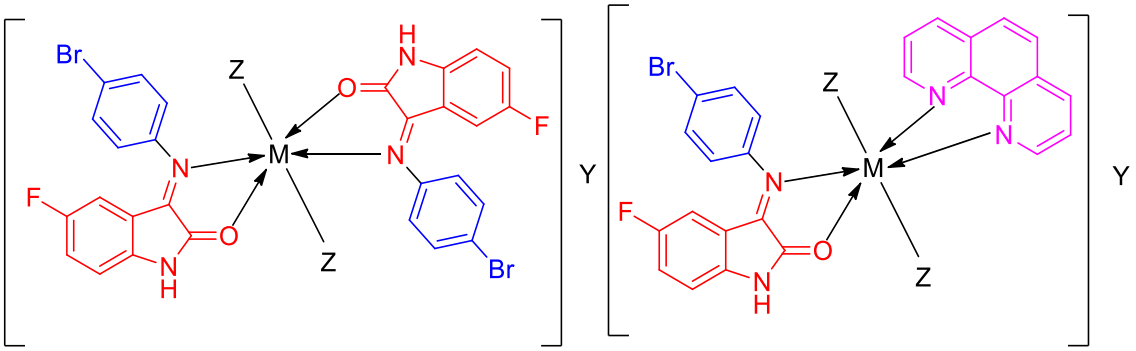

Where M= Cu(II), Ni(II), Co(II), Ru(II) Y=Cl_2, Z= H_2O

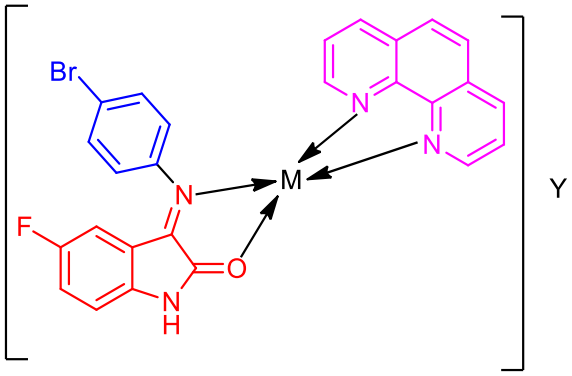

Where M= Cu(II), Y= Cl_2

Scheme 2. Synthesis of metal complexes.

2.2. Antidiabetic activity.

2.2.1. Inhibition assay for amylase activity.

The inhibition of amylase activity was carried out by following the method of Kwone et al. [21]. A total of 500µL of a test sample and 500µL of 0.02M sodium phosphate buffer containing 20 µL of amylase (0.5 mg/ml) were incubated at 25°C for 10 min. After pre-incubation, 500µL of 1% starch solution in 0.02M sodium phosphate buffer (pH 6.9) was added to each tube and incubated for 15 minutes. The reaction was stopped with 1.0 mL of dinitrosalicyclic acid. The test tubes were then incubated in a boiling water bath for 5 min and cooled to room temperature. The reaction mixture was then diluted after adding 10 ml of distilled water, and the absorbance was measured at 540nm.

2.2.2. Inhibition assay for glucosidase activity.

The glucosidase inhibition assay was carried out by following the method of Sheikh et al. [22]. One ml of phosphate buffer (100 mM, pH 6.8) and 80µL of a test sample in different concentrations were mixed with 20 µL of α-Glucosidase (0.01 mg/mL) and incubated at 37°C for 10 min. Next, 50 µL of 5 mM p-nitrophenyl-α-D-glucopyranoside (pNPG) was added to the mixture to start the reaction. The reaction mixture was incubated at 37 °C for 60 min and stopped by adding 2.5 mL of 0.1 M Na_2CO_3. The α-glucosidase activity was determined by measuring the absorbance at 400 nm. Mean values were obtained from triplicate experiments. Inhibition of enzyme activity was calculated as:

$$(\%) = (A\text{-}C) \times 100/ (B\text{-}C),$$

where, A = Sample, B = Blank, and C = Control reading.

2.3. Anticancer activity.

Human cancer cell lines viz HepG2 (Liver) and MDA-MB 231 (Breast) Cells were seeded (1X105 cells/well in triplicate) in a 96-well flat-bottom plate (Becton-Dickinson Lab ware) a day before treatment and grown. Stocks of all compounds (1.0 mg/mL) were made with 5% DMSO (Sigma-Aldrich), and further working solutions (100 µg/mL) were prepared in serum-free culture media. Cells were treated with four doses (6.2, 12.5, 25, and 50 µg/mL in triplicate) of the compounds in complete growth media, including the reference drug, and were further incubated for 48 hours.

2.3.1. Cell proliferation and viability assay.

On day 2 of treatment, cell proliferation and viability tests were performed using the TACS MTT Cell Proliferation and Viability Assay Kit (TACS) as per the manufacturer's instructions. The relationship between surviving compound concentration was plotted to obtain the survival curve of cancer cell lines. The response parameter calculated was the IC_{50} value, which corresponds to the concentration required for 50% inhibition of cell viability.

2.4. DNA damage protection assay.

The DNA damage inhibition by the extract was tested by following the method of [23]. The pBR322 plasmid DNA was subjected to photolysis in the presence of H_2O_2 and UV radiation. The extent of DNA damage was visualized and examined by agarose gel electrophoresis. The following steps were taken to prepare the reaction mixture: In a total volume of 20 µL, hydrogen peroxide (2 µL of 5 mM) was added to a mixture of 0.5 µL of supercoiled plasmid DNA (0.25 µg/µl) and 5 µl of 50 µM of each sample dissolved in $CHCl_3$, followed by dilution with 50 mM Tris-HCl buffer (pH = 7.2). Before performing the electrophoresis experiment, each reaction mixture was incubated at 35°C for 1.5 hours. The samples were then electrophoresed at 80 V for 2 hours on 1.25% agarose gel in tris-acetic acid-EDTA buffer (pH = 8.1). The gel was stained with 1 µg/cm^3 ethidium bromide after electrophoresis (EB). Under UV light, the gel was seen to reveal the cleavages, which were then photographed.

2.5. Molecular docking studies.

The binding modes of α-amylase and α-glucosidase enzymes with synthesized complexes were investigated with the help of molecular docking using the UCS Chimera 1.16 and Biovia discovery studio software to know the different interactions between ligand and protein [24]. The 3D structure of the ligands and their complexes were drawn in the Marvin JS tool (Marvin sketch), and energy minimization was done and saved in PDB format. The 5NN5.pdb, 4GQR.pdb, and 3KJF.pdb files were downloaded from the RCSB Protein data bank for the structure of α-amylase, α-glucosidase, and cancer mutant protein, respectively. These files were processed for energy minimization, and polar hydrogens were added to the UCSF Chimera tool and ready for docking [25]. The docked files were processed using Biovia Discovery Studio software was employed to visualize the docked poses. All the molecules have been docked to the active site of 5NN5 and 4GQR mutant protein. The binding affinity of the complexes was observed as a negative score with a unit of kcal/mol.

3. Results and Discussion

3.1. Physico-chemical characterization.

In general, the complexes were obtained by refluxing respective transition metal salts with ligand and mixed ligand 1,10-phenanthroline at 70°C for 3 hrs in an oil bath with constant magnetic stirring. All the synthesized metal complexes are colored, thermally stable, and insoluble in polar and non-polar solvents except DMSO and DMF. The ligand and metal complexes were analyzed using various physio-chemical properties, melting point, yield, color, elemental analysis, and conductivity measurements. The data is shown in Table 1. The molar conductance value showed that the metal complexes were non-electrolytic. All the metal

complexes were characterized by spectral techniques like FT-IR, UV-visible, mass, powder XRD, EPR for Copper metal complex, and SEM analysis. The analytical data of ligand and metal complexes are in good agreement with their proposed formula.

Table 1. Molecular formulae, color, yield, melting point, elemental analysis, and molar conductance data of metal complexes 6(a-h).

Sl. No.	Complexes	Yield (%)	M.P (°C)	Color	Mol. Wt.	Elemental analysis Calc. (found) (%)				Ohm^{-1} cm^{-2} mol^{-1}
						C	H	N	M	
1	$[Cu(L6)_2(H_2O)_2](Cl_2)$ **(6a)**	81	280	Dark brown	737.80	42.28 (42.13)	2.81 (2.90)	6.80 (6.75)	7.71 (7.72)	36
2	$[Cu(L6)(PT)](Cl_2)$ **(6b)**	78	314	Yellowish green	616.90	49.27 (49.17)	2.54 (2.49)	8.84 (8.66)	10.03 (9.82)	38
3	$[Ni(L6)_2(H_2O)_2](Cl_2)$ **(6c)**	80	294	Red	732.95	42.53 (41.81)	2.83 (2.68)	6.84 (6.82)	7.17 (7.08)	44
4	$[Ni(L6)(PT)(H_2O)_2](Cl)_2$**(6d)**	75	286	Reddish brown	610.05	47.69 (46.81)	3.41 (3.21)	8.24 (8.20)	8.63 (8.58)	42
5	$[Co(L6)_2(H_2O)_2](Cl_2)$ **(6e)**	89	306	Brown	733.19	42.52 (42.48)	2.83 (2.76)	6.84 (6.75)	7.19 (7.10)	48
6	$[Co(L6)(PT)(H_2O)_2](Cl)_2$**(6f)**	85	292	Light brown	610.84	47.67 (47.54)	3.41 (3.37)	8.24 (8.19)	8.66 (8.61)	45
7	$[Ru(L6)_2(H_2O)_2](Cl)_2$**(6g)**	76	326	Black	845.33	40.44 (40.46)	2.69 (2.61)	6.50 (6.54)	11.73 (11.68)	55
8	$[Ru(L6)(PT)(H_2O)_2](Cl)_2$ **(6h)**	69	302	Black brownish	724.36	4.89 (44.81)	3.21 (3.14)	7.76 (7.85)	13.99 (13.79)	58

3.2. FT-IR spectral data.

The infrared spectra of synthesized Schiff base ligand and their metal complexes were collected in the region 4000-400 cm^{-1} to analyze the type of ligand and ligand-metal ion bonding. When metal complexes are chelated, the peak intensities shift to a lower wavenumber than the ligand. The IR spectral bands of ligand and its metal complexes are given in Table 2. The IR spectrum of the Schiff base ligand displayed a strong band at 1738 cm^{-1} due to the C=O amide group. The amide C=O of the ligand was displaced by 6-45 cm^{-1} to a lower frequency of 1693–1731 cm^{-1} in metal complexes, demonstrating the coordination of the ligand's carbonyl oxygen to the metal ion during complexation [26].

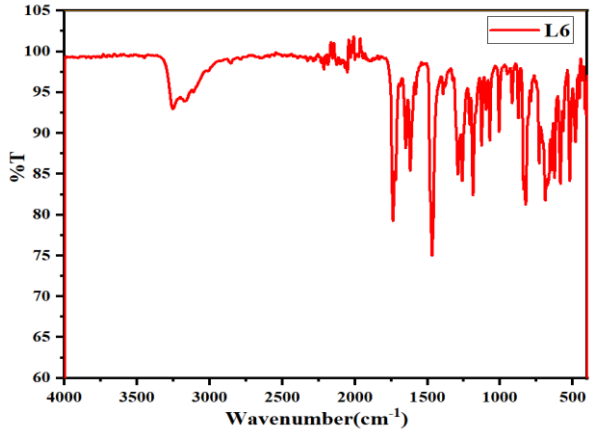

Figure 1. IR spectrum of Ligand (L6).

A broad band of medium intensity is observed at 3258-3067 cm^{-1} due to indolic ν(N-H) [27]. The strong band observed at 1619 cm^{-1} is characterized byν (C=N) of the imine group.

In complexes, the imine of a ligand is shifted to a lower frequency at 5-36 cm^{-1} in the range 1583-1611 cm^{-1} upon coordination with the metal [28]. The metal complexes showed a broad band at 3693-2821 cm^{-1}, the characteristic of (OH) coordinated water molecules. The IR spectra of ligand and metal complexes are shown in Figures 1-2.

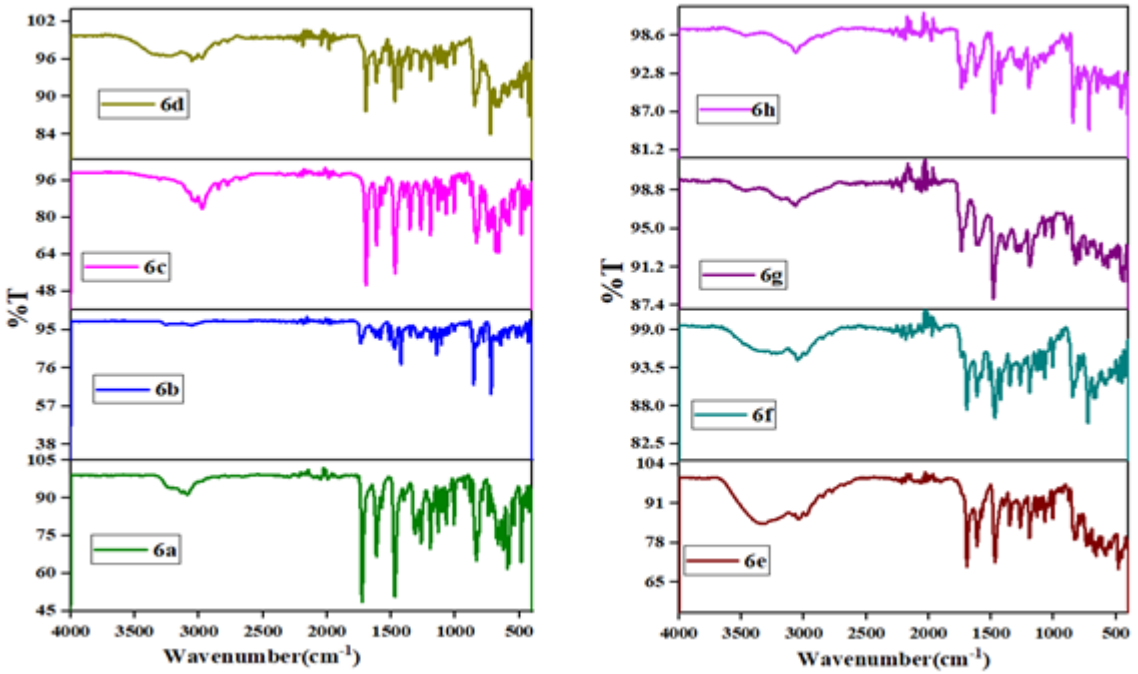

Figure 2. IR spectrum of metal complexes (6a-6h).

Table 2 The important infrared frequencies (in cm^{-1}) of the ligand and its metal complexes**6(a-h).**

Sl. no	Complexes	C=O	C=N	H_2O	M-N	M-O
1	L6	1738	1619	-	-	-
2	6a	1726	1614	3300	480	580
3	6b	1732	1583	-	420	523
4	6c	1695	1611	3154	484	550
5	6d	1696	1610	3642	425	594
6	6e	1697	1623	3693	481	582
7	6f	1693	1609	3609	479	590
8	6g	1731	1599	3624	455	564
9	6h	1704	1612	3110	458	570

3.3. ESR Spectra and magnetic susceptibility measurements.

The electronic spectra were recorded in 10^{-3} M DMSO solution in the range of 200-800 nm at room temperature. The geometry of metal complexes was obtained from the electronic spectra and magnetic susceptibility measurements. The data are represented in Table 3. In the ligand spectrum, two bands were observed. The first band was perceived at 316 nm and is accredited to the π-π* transition of the aromatic ring, and the second band at 442 nm is attributed to the n-π* transition of the azomethine group. In complexes, this band is shifted due to the coordination of azomethine nitrogen with the metal ion, and these bands are observed at 426-484 nm. The electronic spectrum of Cu(II) complexes displays 3 bands at 288,426 nm, and a broad band at 718 nm is a metal-centered d-d transition of distorted octahedral geometry, which can be attributed to $^2B_{1g}\rightarrow{}^2B_{2g}$ and $^2B_{1g}\rightarrow{}^2E_g$ transitions. The magnetic moment of copper complexes was found to be 1.85 B.M, which indicates an octahedral geometry and mixed ligand copper complexes exhibit a band at 426 nm corresponding to $^2B_{1g}\rightarrow 2A_{1g}$ suggests a distorted square planar geometry [29]. In cobalt complexes, the highest intensity band

observed at 328-336 nm may be assigned as L-M charge transfer transition and low intense bands at 450-448 nm correspond to $^4T_{1g}(F)\rightarrow{}^4T_{2g}(P)$ and $^4T_{1g}(F)\rightarrow{}^4A_{2g}$ (F) transition respectively [30]. The magnetic moment was found to be 4.5 B.M. The data suggest the cobalt complexes are octahedral geometry. The nickel complexes display a band at 292, 328-330 nm, and 426-446 nm due to $^3A_{2g}\rightarrow{}^3T_{2g}$, $^3A_{2g}\rightarrow{}^3T_{1g}(F)$, and $^3A_{2g}\rightarrow{}^3T_{1g}(P)$ respectively, and the magnetic moment was 3.09 which indicates an octahedral geometry [31]. In complexes, the bands at 330-340 nm, 420-450 nm, and 516-616 nm are assigned to $^4T_{1g}(F)\rightarrow{}^4T_{2g}$ (F), $^4T_{1g}\rightarrow{}^4A_{2g}(F)$, $^4T_{1g}$ (F)$\rightarrow{}^4T_{1g}$ (P) magnetic moment was 4.96 BM suggests an octahedral geometry [32]. The ESR spectrum of ligand and metal complexes is shown in Figure 3.

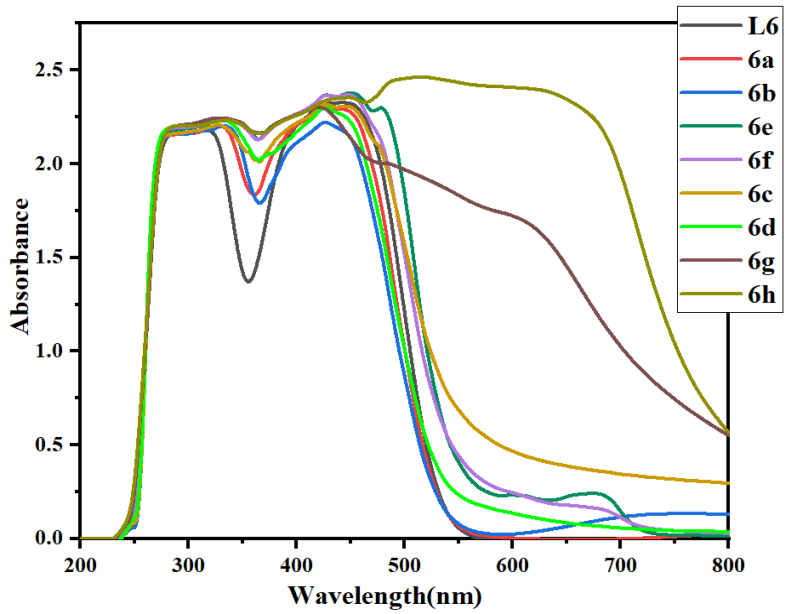

Figure 3. Electronic spectra of Ligand (L6) and its complexes (6a-6h).

Table 3. Electronic spectral data of synthesized ligand and its complexes 6(a-h) along with their absorption band.

Sl. no	Complexes	Frequencies (nm)	Absorption band	$U_{effective}$ (B.M)	Geometry
1	L6	316, 442	π–π*, n-π*	-	-
2	6a	286, 426	$^2B_{1g}\rightarrow{}^2B_{2g}$ $^2B_{1g}\rightarrow{}^2E_g$	1.86	Octahedral
3	6b	288, 426, 718	$^2B_{1g}\rightarrow2A_{1g}$	1.83	Distorted square planar
4	6c	328 446	$^3A_{2g}\rightarrow{}^3T_{1g}$ (F) $^3A_{2g}\rightarrow{}^3T_{1g}$ (P),	3.21	Octahedral
5	6d	330 426	$^3A_{2g}\rightarrow{}^3T_{1g}$ (F) $^3A_{2g}\rightarrow{}^3T_{1g}$ (P),	3.28	Octahedral
6	6e	328 450 678	$^4T_{1g}$ (F)$\rightarrow{}^4T_{2g}$ (F), $^4T_{1g}$ (F)$\rightarrow{}^4A_{2g}$ (F) $^4T_{1g}$ (F)$\rightarrow{}^4T_{1g}$ (P)	3.92	Octahedral
7	6f	332 448 681	$^4T_{1g}$ (F)$\rightarrow{}^4T_{2g}$ (F), $^4T_{1g}$ (F)$\rightarrow{}^4A_{2g}$ (F) $^4T_{1g}$ (F)$\rightarrow{}^4T_{1g}$ (P)	3.86	Octahedral
8	6g	330 420 616	$^4T_{1g}(F)\rightarrow{}^4T_{2g}(F)$ $^4T_{1g}\rightarrow{}^4A_{2g}(F)$ $^4T_{1g}$ (F)$\rightarrow{}^4T_{1g}$ (P)	5.83	Octahedral
9	6h	290 428 516	$^4T_{1g}(F)\rightarrow{}^4T_{2g}(F)$ $^4T_{1g}\rightarrow{}^4A_{2g}(F)$ $^4T_{1g}$ (F)$\rightarrow{}^4T_{1g}$ (P)	5.88	Octahedral

3.4. NMR spectroscopy.

The ^{1}H NMR spectrum of ligand was recorded in DMSO-d6 using trimethylsilane as a reference standard. The NMR of the ligand exhibited a singlet at 10.99 ppm (s, 1H), which was assigned to the NH proton of the indole ring. The aromatic protons of the ligand were observed as multiplet in the range of 6-87-7.51 ppm (m, 7H). The ^{13}C NMR of ligand appears as a signal at δ=163.93 ppm is attributed to the carbon of the azomethine group (CH=N), and the peak at 159.17 ppm corresponds to the carbon of the amide group. The peaks observed betweenδ=110.38-158.56 ppm show the aromatic ring carbons. The ^{1}H NMR and ^{13}C NMR spectra of the ligand are given in Figure S1 and Figure S2.

3.5. Mass spectroscopy.

The mass of the Schiff base ligand showed a molecular ion peak at 319.82m/z. The mass spectra of complexes showed molecular ion peaks exhibited at m/z 735 (6a), 614 (6b), 734 (6c), 575 (6d), 732 (6e), 593 (6f), 735(6g), 636.43(6h) respectively. The mass spectrum of ligand and metal complexes is depicted in Figure S6- S14.

3.6.EPR spectra.

At ambient temperature (300K), the copper metal complexes of ESR spectra X-band revealed axial patterns since they are magnetically concentrated, and hyperfine splitting was unclear in both parallel and perpendicular regions(^{63}Cu, I=3/2). The g value was calculated from the spectra of the Cu(II) complex (Figure 4). The analysis of the spectrum gives g∥ =2.1749, and g⊥= 2.0943. The trend g∥> g⊥observed in these complexes indicates that the Cu(II) is tetragonally elongated along the z-axis, indicating a distorted octahedral coordination environment, and the unpaired electron most likely resides predominantly in the d_{x2-y2} orbital (g∥> g⊥> 2.0) of the Cu(II) ion and is the characteristic feature for the axial symmetry [33]. The deviation of "g" values from the free electron value (2.0023) is by angular momentum contribution in the complexes.

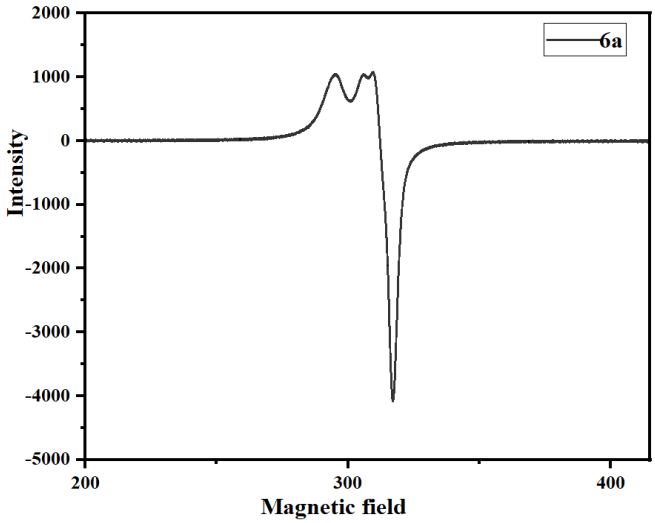

Figure 4. EPR Spectrum of copper complex (6a).

The g∥ value is less than 2.3, which indicates an appreciable covalent character for the metal-ligand bond. The average "g" value for overall distortion is calculated using the equation: g_{avg} = (1/3)(2g⊥ + g∥) g_{avg} =2.1211. The geometric parameter (G) measures the extent of the

exchange interaction and is calculated using g-tensor values by the expression G= g∥ -2/g⊥ -2. Hathway and Billing claim that if the G value is more than 4, the exchange interaction between copper centers is minimal, whereas if the G value is less than 4, the exchange interaction is noticeable. [34]. The calculated G value for 6a is 1.85, indicating that exchange coupling effects are present in the complex.

3.7. Powder XRD.

The size, amorphousness, and crystal structure of the metal complexes were investigated using powder X-ray diffraction analysis. X-ray diffraction analysis is used to understand the crystal structure of metal complexes. The crystal structure of a substance, or more precisely, the size and shape of the unit cell, which defines the angular positions of the relative intensities of the lines, typically determines its diffraction pattern [35]. Since the diffraction pattern depends on the structure, one can infer the structure from the diffraction pattern. The complexes were examined for temperatures between 5 and 700 °C. The powder XRD pattern of metal complexes is shown in Figure 5. The average particle size of samples was estimated by using Debye Scherrer's equation:

$$D = 0.9\lambda/\beta \cos\theta$$

where θ is the Bragg diffraction angle for the hkl plane, β is the full-width half maximum (FWHM) of the characteristic peak, λ is the wavelength (1.54 A) of the X-ray source used in XRD

The average grain size of metal complexes was calculated as **6a** is 80.91nm and **6e** is 81.22nm.

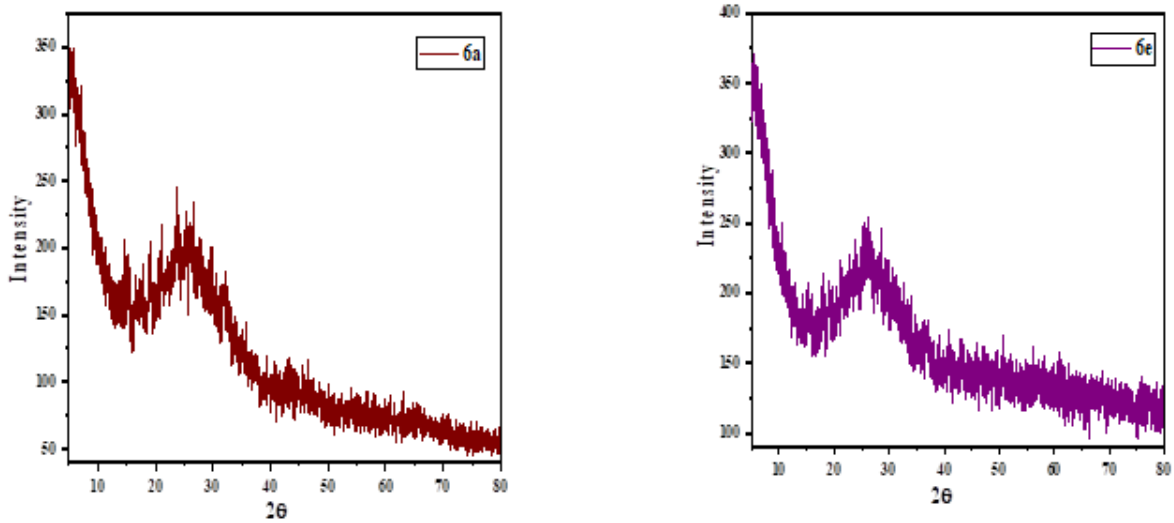

Figure 5. Powdered XRD spectrum of 6a and 6e.

3.8. TGA analysis.

The complexes' thermal analysis was studied using a thermogravimetric technique within the temperature range from room temperature to 800°C at a heating rate of 10°C/min. The thermal decomposition of complexes 6a undergoes three stages. The first stage is a degradation step where weight loss of 2.23% in the temperature range of 61–166°C with DTG peaks at 105°C was observed in a complex. This weight loss is due to the liberation of a chlorine atom. The second stage degrade at the temperature range of 170–218°C by losing coordinated water molecules with a weight loss of 3.7% with DTG peaks observed at 236°C. This complex's third stage of decomposition occurred at the temperature range of 230–570°C with a weight

loss of 35% due to the loss of ligand moiety with DTG peak observed at 270 and 532°C. The metallic residue left has an observed weight of 41% [36]. The 6e complex undergoes decomposition in two stages. The first stage occurred at the temperature range of 54-144°C with a weight loss of 2.61%. This weight loss corresponds to the loss of Cl2 molecules with a DTG peak observed at 242°C. The second stage of degradation occurred at the temperature range of 154–596°C with a weight loss of 42%. This weight loss corresponds to the simultaneous loss of water molecules and ligands with DTG peaks observed at 296, 325, and 597°C. The metallic residue finally left has the observed mass of 38% [37]. The diagram is depicted in Figure 6**.**

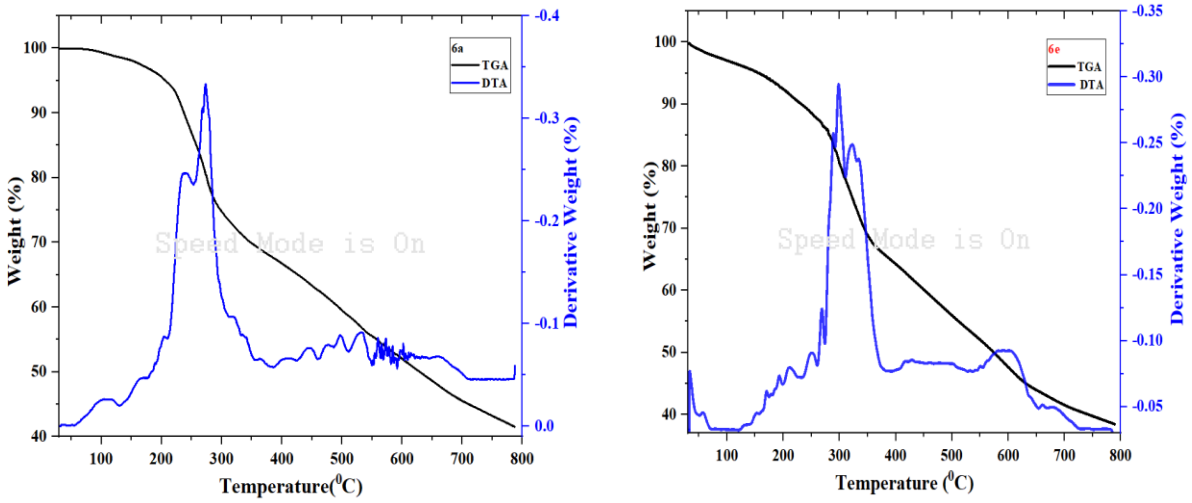

Figure 6. TGA spectrum of (6a and 6e).

3.9. SEM analysis.

The Schiff base ligand and their metal complexes of surface morphology were studied by using scanning electron microscope (SEM) analysis. The isatin Schiff base ligand shows long spikes as particles are observed. The 6a metal complex shows a rod-like structure, and the 6e metal complex agglomerated roots-like particles are observed. Due to the complexation and metal ions, the surface morphology of SEM micrographs revealed that the metal complexes differ from ligands each other. Photography of SEM is depicted in Figure 7.

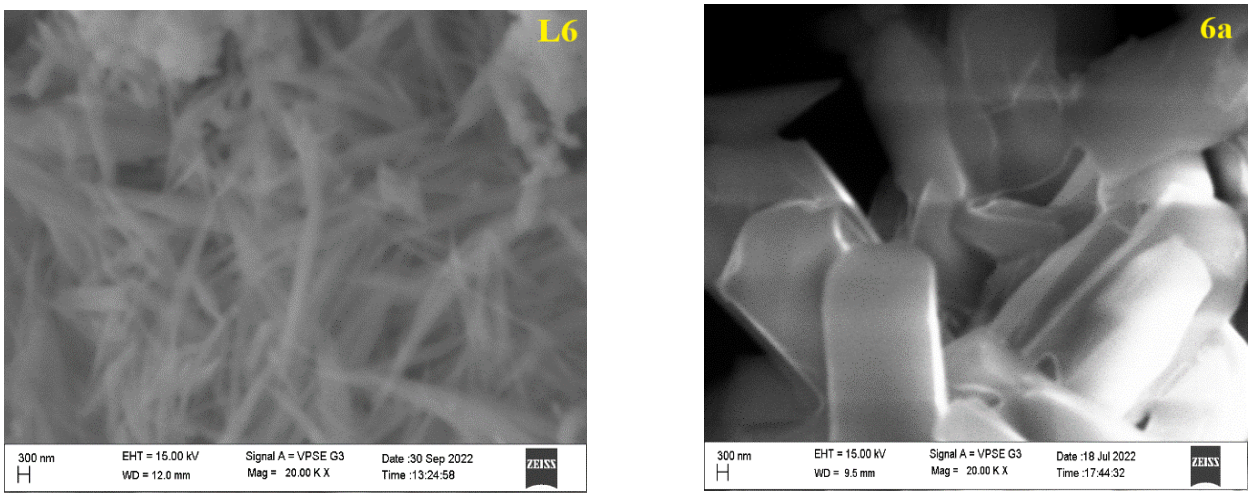

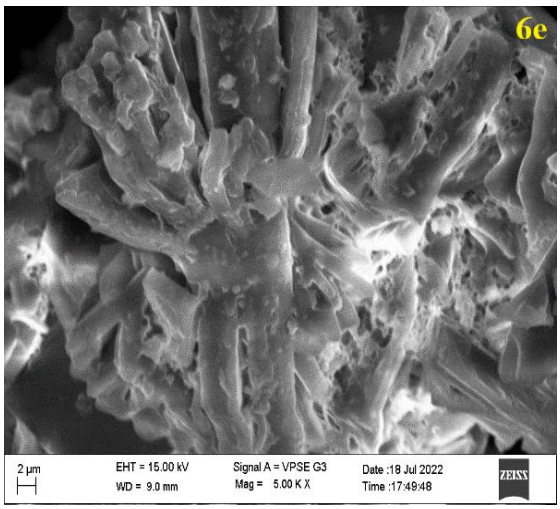

Figure 7 SEM images of ligand (**L6**), **6a** and **6e**.

3.10. Antidiabetic assay.

The hydrolysis of α-1,4-glycosidic bonds in starch and other polysaccharides by the enzyme alpha-amylase produces a variety of smaller sugar molecules, including maltose and glucose. Diabetes develops when the body produces too many of these little sugar molecules as a result of the breakdown of polysaccharides by the enzyme amylase. Therefore, it is essential to control the activity of (-amylase) to prevent postprandial hyperglycemia (PPHG). The percent inhibition ranged from 25 to 72% at a 500 ug/mL concentration. The activity result is shown in Figure 8. Initially, a ligand shows certain activity due to the presence of an electron-withdrawing group and a hydroxy group. Upon complexation with metal ions, its enhancement in activity was observed. The compound 6e shows excellent α-amylase activity compared to standard acarbose. Increased conjugation and the presence of a π-cloud may be the cause of the complexes' improved activity. The amylase enzyme's active site is known to be situated in a V-shaped depression on its surface. Hydrogen bonds or other hydrophobic interactions may be used to bind the active site or another site close to it in the complexes [38]. In the present study, compound 6f (68%) shows the highest activity compared to the free ligand. This might be due to the electrostatic interaction between the positively charged complex molecules and the negatively charged N/O containing ligand moiety, which would force the complex molecules into proximity, causing the complex molecules to aggregate through metal-metal or π-πinteraction. This electrostatic interaction causes effective changes in alpha-glucosidase activity, and the complexes' attachment to the enzymes' oxygen atoms may cause their suppression of activity. The electrostatic property of complexes increases, which leads to the growth of the MLCT absorption band at different wavelengths [39]. Therefore, the complex may discover that the ligand has less significance than it does in the creation of new oral diabetic medications. These substances typically have an effect on these metabolic enzymes at the micromolar level [40]. As a result, these substances are essential for making drugs. As is well known, several glucosidase inhibitors have powerful antidiabetic effects. A healthy diet high in fat and carbohydrates, weight loss, regular exercise, the use of oral hypoglycemic medications, and insulin injections are the most efficient ways to help patients with type 2 diabetes mellitus (T2DM) improve their glucose control. Treatments for T2DM often involve oral hypoglycemic agents such as miglitol, acarbose, and voglibose. For instance, in our study, we preferred acarbose as the standard [41].

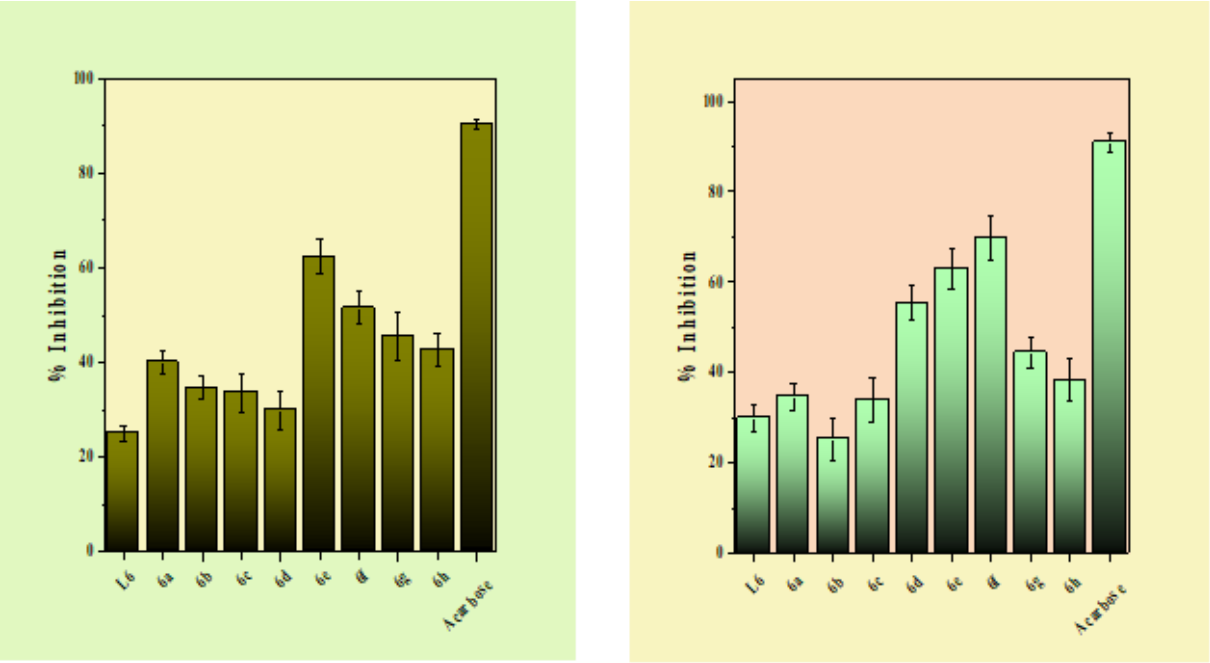

a) b)

Figure 8. Antidiabetic activity **a)** α–amylase activity,**b)**α–glucosidase activity.

3.11. Anticancer activity.

The anticancer activity of the ligand and its complexes were studied against the HepG2 cell line and MDA-MB-231 cell lines. The percentage activity is the measurement of % in vitro cell inhibition by using MTT colorimetric assay. The ligand and metal complexes were analyzed in various concentrations. The anticancer activity of synthesized isatin Schiff base ligand and its metal complexes are shown in Figure 9**.** The results are expressed in IC_{50} values, and 5-fluorouracil was used as the standard. The IC_{50} value of complex 6f shows the highest promising cytotoxic activity compared to other complexes. The cobalt complexes can make cancer cells undergo apoptosis in vitro in a concentration-dependent way, inhibiting the propagation of HepG2 cancer cells. Notably, only a few reports were available on the cytotoxicity of isatin metal complexes against the HepG2 cell line and MDA-MB-231 cell lines.

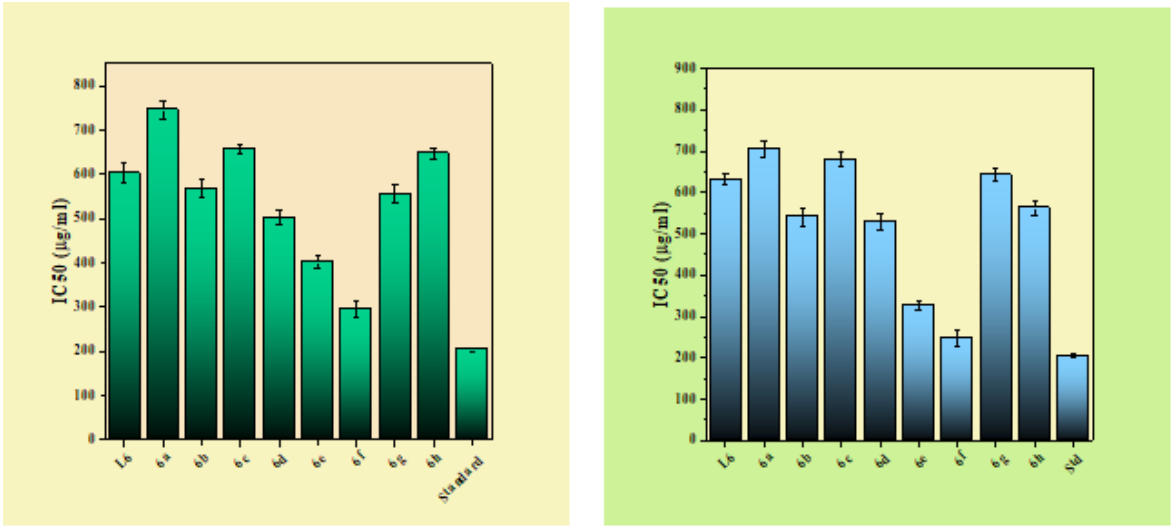

a) b)

Figure 9. Anticancer activity **a)** MDA-MB 231 cell line **b)** HepG2 cell line..

3.12. DNA cleavage.

The metal complexes of DNA cleavage activity in the presence of H_2O_2 have been investigated, and the results are shown in Figure 10. In the control experiment using DNA alone (Lane 2), no significant cleavage occurs. It is evident from the figure that the 6e metal complex shows more cleavage than the other selected complexes in the presence of H_2O_2. However, when the concentration was increased, 6g also showed more cleavage. This is due to the hydroxyl radical production being increased and reacting H_2O_2 with the metal ion. The transfer of pBR322 DNA from its naturally occurring circularly closed covalent form (form I) to the nicked circular form (form II) after incubation with a metal complex was seen using an electrophoretic gel technique. During the incubation time, these transitions will be seen for all complexes, regardless of the concentration of the sample solution. DNA cleavage efficiency of complexes in gel agarose media can be quantitatively measured by relaxing supercoiled pBR322 DNA into nicked and linear form (form II). Metal complex intercalation with DNA can reduce the mobility of the supercoiled form, which can be seen separately as an ultraviolet photographic image. However, the supercoiled form of pBR322 is not considerably affected by weak electrostatic contact. Hence, there is no change in its mobility rate under a gel medium [42].

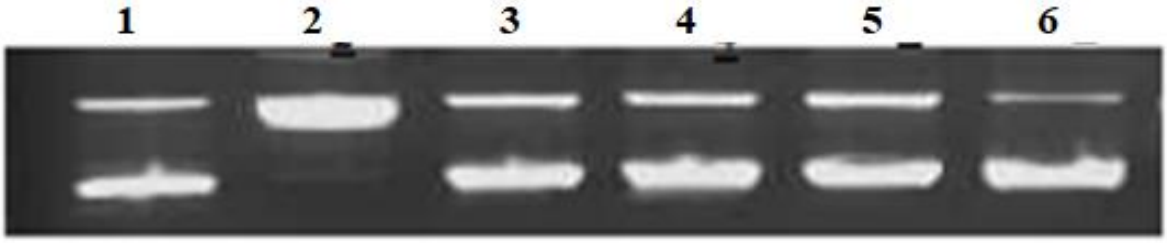

Figure 10.Cleavage of supercoiled pBR322 DNA (0.5 µg) by the Co(II), Ni(II), Cu(II), and Ru(III) complexes in a buffer containing 50 mM Tris-HCl and 50 mMNaCl at 37°C. Lane 1: DNA + 40 µl of 6e, Lane 2: DNA alone, Lane 3: DNA + 40 µl of 6a, Lane 4: DNA + 40 µl of 6d, Lane 5: DNA + 40 µl of 6g, Lane 6: DNA + 60 µl of 6g.

3.13 Molecular docking studies.

The docking analysis of ligand and cobalt metal complex (6e) was analyzed and found to reveal a good interaction with protein. The interaction with the binding site is displayed in Figures 11-12, and docking energies are given in Table 4. The docking result of human pancreatic α–amylase (PDB ID: 4GQR) with ligand showed residues of TYR 62, LEU 165, ASP 300, and 2 hydrogen bonds with ARG 195, GLU235 with a bond length of 1.98A°. The **6e** metal complex shows a hydrogen bond with PRO 332 (3.27A°) and LYS 457 (2.28 A°), GLY334 (2.10 A°), and the binding energy is -8.7 kcal/mol. Similarly, the docking result of α–glucosidase (PDB ID: 5NN5) with ligand shows various bonds such as pi-pi, hydrogen bonds TRP 126 (2.79 A°), CYS 127 (2.07A°), ASP 91(2.61A°), ALA 93(2.38A°), ALA 97, LYS 96. The result of the hydrogen bond interaction of 6e indicates a significant binding with GLN 776(2.06A°), NH of indole binds with VAL 778(2.23A°), ILE 780(2.90A°), and hydroxyl of O atom with ILE 780(1.94A°). The docking result of 3KJF with ligand showed a hydrogen bond with ARG 207(2.43A°) and pi-alkyl bond TYR 204, PHE 256. Similarly, the presence of hydrogen bond on O atom GLU 248(2.84A°) with the hydroxyl of O atom, NH of a compound with SER 249(2.48A°), GLU 248(2.60A°) and the binding energy is -9.1 kcal/mole. Thus, it indicates that the metal complex 6e is more favorable than the ligand (L6) [43].

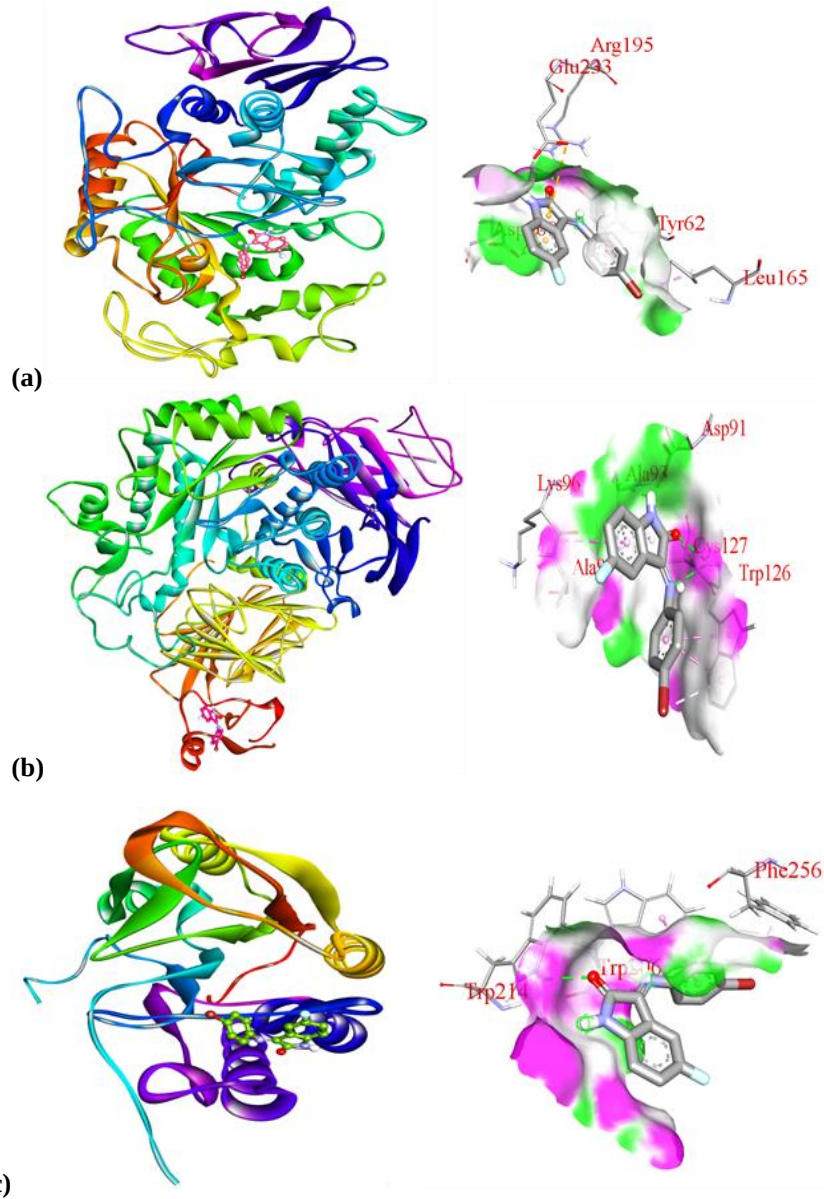

Figure 11. Molecular docking of ligand (L6) with **(a)** α–amylase and active site amino acid residue interactions, **(b)** α–glucosidase and active site amino acid residue interactions, (**c)** 3KJF and active site amino acid residue interactions.

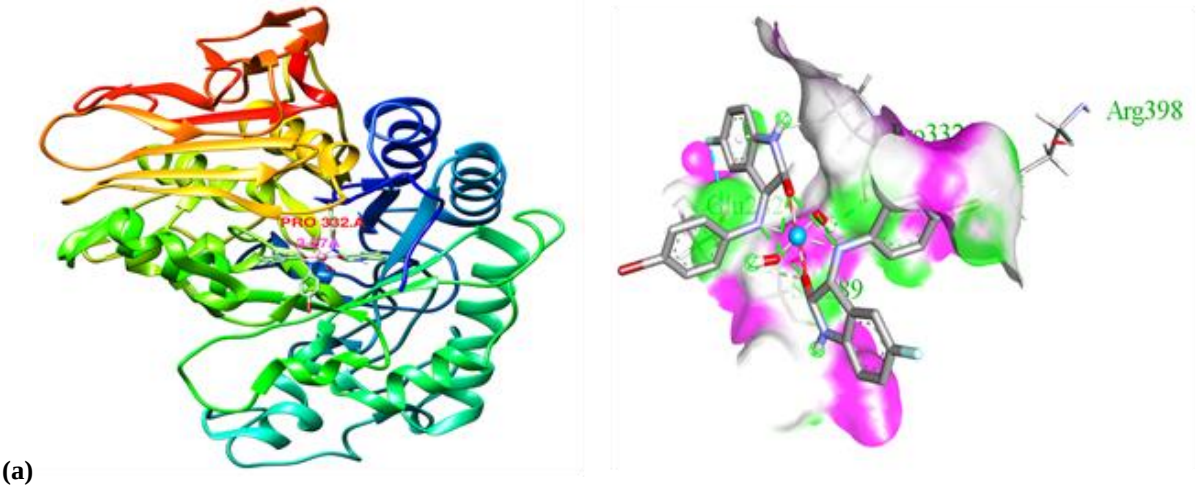

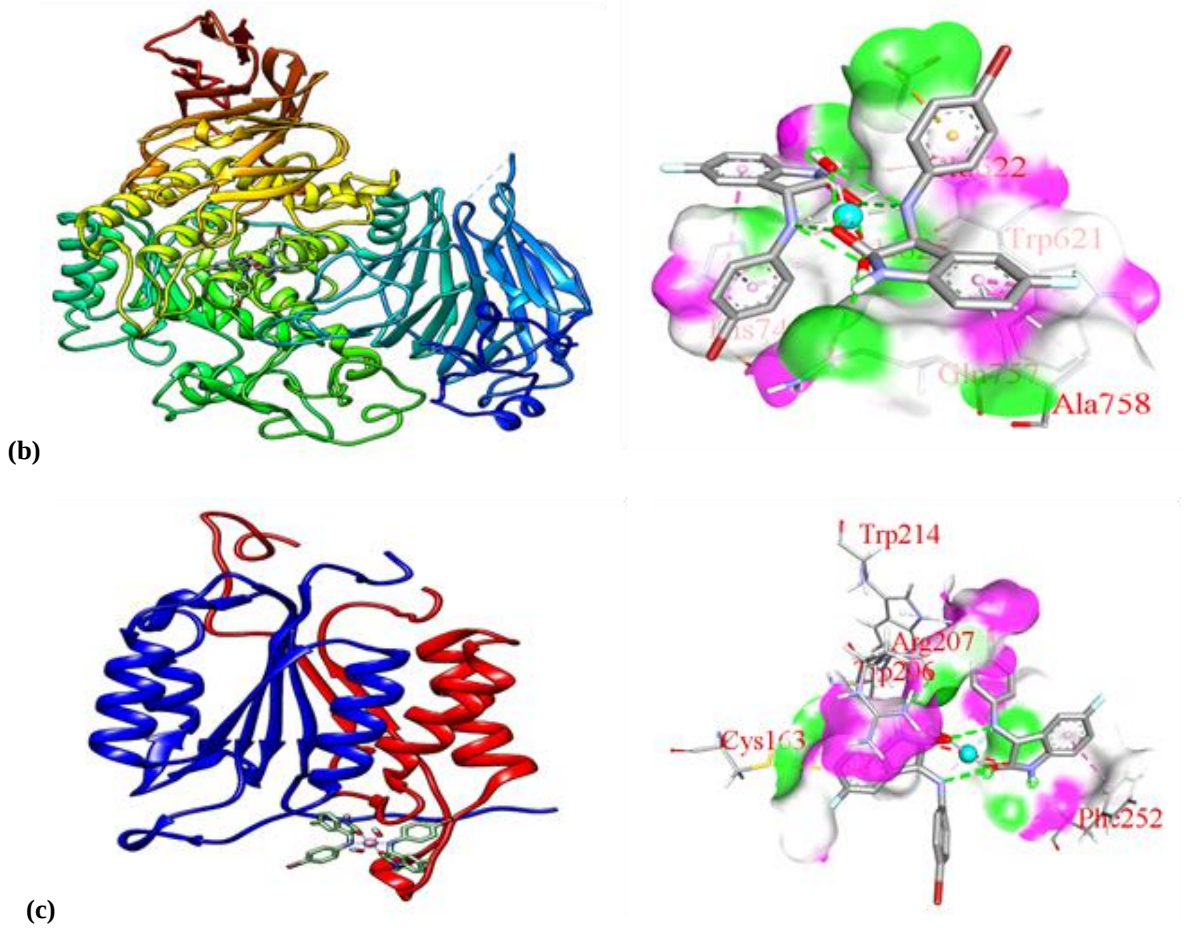

Figure 12. Molecular docking of **6e** with (**a**) **6e** with 4GQR, (**b**) 5NN5 and (**c**) 3KJF.

Table 4 Docking score of ligand (**L6**) and **6e** metal complex.

Compound	4GQR Binding energy (kcal/mol)	5NN5 Binding energy (kcal/mol)	3KJF Binding energy (kcal/mol)
L6	-7.5	-7.3	-6.1
6a	-7.9	-8.6	-6.8
6b	-8.0	-7.4	-8.3
6c	-7.6	-8.1	-7.2
6d	-7.2	-10.1	-8.7
6e	-8.7	-9.8	-9.1
6f	-8.3	-9.9	-9.3
6g	-8.2	-9.5	-8.1
6h	-8.1	-9.0	-7.6

4. Conclusions

Metal complexes (6a-6h) of the isatin Schiff base ligand L6 were synthesized and characterized. The molar conductance data showed that the complexes are electrolytic. IR spectral data reveals the bidentate nature of the ligand coordinating through the imine nitrogen and oxygen of the carbonyl group (O/N) in complexes. Based on the results obtained from electronic absorption, octahedral geometry has been assigned to the synthesized complexes.^{1}H NMR, ^{13}C NMR, and mass spectral data support the structure of L6 and the complexes. Antidiabetic study reveals that complex 6e has the highest activity in α-amylase and 6f in α-glucosidase activity. Complex 6f showed the highest activity as compared to ligands against HepG2 (Liver) and MDA-MB 231. DNA cleavage studies have shown that the complexes can cleave nucleic acids, and the extent of the cleavage is found to be dose-dependent. The molecular docking of metal complex 6e is more favorable than the ligand (**L6**).

Funding

One of the authors, Ms. Neelufar owes her sincere gratitude to the University Grants Commission ((F. No.16-6(DEC.2017)/2018(NET/CSIR)),) New Delhi (India) for the award of Junior Research Fellowship under the UGC-JRF-Fellow.

Acknowledgments

The authors thank the Institute of Excellence, Vijnana Bhavana, University of Mysore, Manasagangotri, Mysuru, for providing us with spectral data.

Conflicts of Interest

The authors declare no conflict of interest.

References

1. Mishra, R.; Chaurasia, H.; Singh, V.K.; Naaz, F.; Singh, R.K. Molecular modeling, QSAR analysis and anti-microbial properties of Schiff base derivatives of isatin. *J. Mol Struct.* **2021,** *1243*, 130763, https://doi.org/10.1016/j.molstruc.2021.130763.
2. Fayed, E.A.; Eldin, R.R.E.; Mehany, A.B.M.; Bayoumi, A.H.; Ammar, Y.A. Isatin-Schiff's base and chalcone hybrids as chemically apoptotic inducers and EGFR inhibitors; design, synthesis, anti-proliferative activities and in silico evaluation. *J. Mol. Struct.* **2021**, *1234*, 130159, https://doi.org/10.1016/j.molstruc.2021.130159.
3. Davidovich, P.; Novikova, D.; Tribulovich, V.; Smirnov, S.; Gurzhiy, V.; Melino, G.; Garabadzhiu, A. First X-ray structural characterization of isatin Schiff base derivative. NMR and theoretical conformational studies. *J. Mol. Struct.* **2014**, *1075*, 450–455, https://doi.org/10.1016/j.molstruc.2014.07.008.
4. Ghosh, S.; Ramarao, T.A.; Samanta, P.K.; Jha, A.; Satpati, P.; Sen, A. Triazole based Isatin derivatives as potential inhibitor of key cancer promoting kinases- insight from electronic structure, docking and molecular dynamics simulations. *J. Mol. Graph. Model.* **2021,** *107*, 107944, https://doi.org/10.1016/j.jmgm.2021.107944.
5. Dileepan, A.G. B.; Prakash, T.D.; Kumar, A.G.; Rajam, P.S.; Dhayabaran, V.V.; Rajaram, R. Isatin based macrocyclic Schiff base ligands as novel candidates for anti-microbial and antioxidant drug design: *In vitro* DNA binding and biological studies. *J. Photochem. PhotobioL. B, Biol.* **2018,** *183*, 191–200, https://doi.org/10.1016/j.jphotobiol.2018.04.029.
6. Singh, G.; Kalra, P.; Singh, A.; Sharma, G.; Sanchita; Pawan; Mohit; Espinosa-Ruiz, C.; Esteban, M.A. A quick microwave preparation of isatin hydrazone schiff base conjugated organosilicon compounds: Exploration of their antibacterial, antifungal, and antioxidative potentials. *J. Organomet. Chem.* **2021,** *953*, 122051, http://doi.org/10.1016/j.jorganchem.2021.122051.
7. Sahin, K.; Saripinar, E.; Durdagi, S. Combined 4D-QSAR and target-based approaches for the determination of bioactive Isatin derivatives. *SAR QSAR Environ. Res.* **2021,** *32*, 769-792, https://doi.org/10.1080/1062936X.2021.1971760.
8. Badavath, V.N.; Kumar, A.; Samanta, P.K.; Maji, S.; Das, A.; Blum, G.; Jha,A.; Sen, A. Determination of potential inhibitors based on isatin derivatives against SARS-CoV-2 main protease (m^{pro}): a molecular docking, molecular dynamics and structure-activity relationship studies. *J. Biomol. Struct. Dyn.* **2022,** *40*, 3110-3128, https://doi.org/10.1080/07391102.2020.1845800.
9. Freitas, L.A.B.; Santos, A.C. da S.; Silva, G. de C.; Albuquerque, F.N. do N.; Silva, E.D.; Simone, C.A. de; Pereira, V.R.A.; Alves, L.C.; Brayner, F.A.; Leite, A.C.L.; Gomes, P.A.T. de M. Structural improvement of new thiazolyl-isatin derivatives produces potent and selective trypanocidal and leishmanicidal compounds. *Chem.-Biol. Interact.* **2021,** *345*, 109561, https://doi.org/10.1016/j.cbi.2021.109561.
10. Brandao, P.; Marques, C.; Burke, A.J.; Pineiro, M. The application of isatin-based multicomponent-reactions in the quest for new bioactive and druglike molecules. *Eur. J. Med. Chem.* **2021,** *211*, 113102, https://doi.org/10.1016/j.ejmech.2020.113102.
11. Yakan, H.; Cavus, M.S.; Kurt, B.Z.; Muglu, H.; Sonmez, F.; Guzel, E. A new series of asymmetric bis-isatin derivatives containing urea/thiourea moiety: Preparation, spectroscopic elucidation, antioxidant properties

and theoretical calculations. *J. Mol. Struct.* **2021,** *1239*, 130495, https://doi.org/10.1016/j.molstruc.2021.130495.
12. Khatoon, S.; Aroosh, A.; Islam, A.; Kalsoom, S.; Ahmad, F.; Hameed, S.; Abbasi, S.W.; Yasinzai, M.; Naseer, M.M. Novel coumarin-isatin hybrids as potent antileishmanial agents: Synthesis, *in silico* and *in vitro* evaluations. *Bioorg. Chem.* **2021,** *110*, 104816, http://doi.org/10.1016/j.bioorg.2021.104816.
13. Tangadanchu, V.K.R.; Sui, Y.F.; Zhou, C.H.; Isatin-derived azoles as new potential anti-microbial agents: Design, synthesis and biological evaluation. *Bioorganic Med. Chem. Lett.* **2021,** *41*, 128030, http://doi.org/10.1016/j.bmcl.2021.128030.
14. Emami, S.; Valipour, M.; Komishani, F.K.; Sadati-Ashrafi, F.; Rasoulian, M.; Ghasemian, M.; Tajbakhsh, M.; Masihi, P.H.; Shakiba, A.; Irannejad, H.; Ahangar, N.; Synthesis, *in silico*, *in vitro* and *in vivo* evaluations of isatin aroylhydrazones as highly potent anticonvulsant agents. *Bioorg. Chem.* **2021,** *112*, 104943, http://doi.org/10.1016/j.bioorg.2021.104943.
15. Hua, L.; Li, W.; Chen, Y.; Liang, K.; Cai, H.; Wang, J.; Wang, S.; Yin, T.; Liang, L. A hexanuclear Nd (III) complex derived from a Schiff base with significant antitumor and antifungal activity. *Appl. Organomet. Chem.* **2021,** *35*, e6081, https://doi.org/10.1002/aoc.6081.
16. Cheke, R.S.; Patil, V.M.; Firke, S.D.; Ambhore, J.P.; Ansari, I.A.; Patel, H.M.; Shinde, S.D.; Pasupuleti, V.R.; Hassan, M.I.; Adnan, M.; Kadri, A.; Snoussi, M. Therapeutic Outcomes of Isatin and Its Derivatives against Multiple Diseases: Recent Developments in Drug Discovery. *Pharm*. **2022,** *15*, 272, https://doi.org/10.3390/ph15030272.
17. Chinnasamy, R.P.; Sundararajan, R.; Govindaraj, S. Synthesis, characterization, and analgesic activity of novel schiff base of isatin derivatives. *J. Adv. Pharm. Technol. Res.* **2010,** *1*,342-347, https://doi.org/10.4103%2F0110-5558.72428..
18. Patil, P.R.; Javarappa, R., Kumar, A.C.; Naik, N. Synthesis of Co(II), Ni(II) and Zn(II) Metal Complexes Derived from a Hydrazone Schiff Base: Electrochemical Behavior and Comprehensive Biological Studies. *Chemistry Select* **2022,** *7*, e202200752, https://doi.org/10.1002/slct.202200752.
19. Neelufar; Rangaswamy, J.; Ankali, K.N.; Naik, N.; Nuthan, B.R.; Satish, S. The Mn (II), Co (II), Ni (II) and Cu (II) complexes of (Z)-N' ((1H-indol-3-yl) methylene) nicotinohydrazide Schiff base: synthesis, characterization and biological evaluation. *J. Iran. Chem. Soc.* **2022**, *19*, 3993-4004, https://doi.org/10.1007/s13738-022-02580-1.
20. Revanna, B.N.; Madegowda, M.; Neelufar; Rangaswamy, J.; Naik, N. A novel Schiff base derivative as a fluorescent probe for selective detection of Cu^{2+} ions in buffered solution at pH 7.5: Experimental and quantum chemical calculations. *J. Mol. Struct.* **2022,** *1254*, 132327, https://doi.org/10.1016/j.molstruc.2021.132327.
21. Kwon, Y.; Shim, H.S.; Wang, X.; Montell, C. Control of thermotactic behavior via coupling of a TRP channel to a phospholipase C signaling cascade. *Nat. Neurosci.* **2008,** *11*, 871-873, https://doi.org/10.1038/nn.2170.
22. Pasha, Z.; Wang, Y.; Sheikh, R.; Zhang, D.; Zhao, T.; Ashraf, M. Preconditioning enhances cell survival and differentiation of stem cells during transplantation in infarcted myocardium. *Cardiovasc. Res.* **2008,** *77*, 134-142, https://doi.org/10.1093/cvr/cvm025.
23. Neelakantan, M.A.; Rusalraj, F.; Dharmaraja, J.; Johnsonraja, S.; Jeyakumar, T.; Pillai, M.S. Spectral characterization, cyclic voltammetry, morphology, biological activities and DNA cleaving studies of amino acid Schiff base metal (II) complexes. *Spectrochim. Acta A Mol. Biomol. Spectrosc.* **2008,** *71*, 1599-1609, https://doi.org/10.1016/j.saa.2008.06.008.
24. Diab, M.A.; Mohammed, G.G.; Mahmoud, W.H.; El-Sonbati, A.Z.; Morgan, S.M.; Abbas, S.Y. Inner metal complexes of tetradentate Schiff base: Synthesis, characterization, biological activity and molecular docking studies. *Appl. Organomet. Chem.* **2019,** *33*, e4945, https://doi.org/10.1002/aoc.4945.
25. Hosny, N.M.; Belal, A.; Motawea, R.; Hussien, M.A.; Abdel-Rhman, M.H. Spectral characterization, DFT, docking and cytotoxicity of N-benzyl-4,5-dihydro-3-methyl-5-oxo-1*H*-pyrazole-4-carbothioamide and its metal complexes. *J. Mol. Struct.* **2021,** *1232*, 130020, https://doi.org/10.1016/j.molstruc.2021.130020.
26. Pervez, H.; Ahmad,M.; Zaib, S.; Yaqub, M.; Naseer, M.M.; Iqbal, J. Synthesis, cytotoxic and urease inhibitory activities of some novel isatin-derived bis-Schiff bases and their copper(II) complexes. *Med. Chem. Commun.* **2016,** *7*, 914-923, https://doi.org/10.1039/C5MD00529A.
27. Dar, O.A.; Lone, S.A.; Malik, M.A.;Aqlan, F.M; Wani, M.Y.; Hashmi, A.A.; Ahmad, A. Synthesis and synergistic studies of isatin based mixed ligand complexes as potential antifungal therapeutic agents. *Heliyon* **2019,** *5*, e02055, https://doi.org/10.1016/j.heliyon.2019.e02055.
28. Nitha, L.P; Aswathy, R.; Mathews, N.A.; Kumari, B.S.; Mohanan, K. Synthesis, spectroscopic

characterisation, DNA cleavage, superoxidase dismutase activity and antibacterial properties of some transition metal complexes of a novel bidentate Schiff base derived from isatin and 2-aminopyrimidine. *Spectrochim. Acta A Mol. Biomol. Spectrosc.* **2014,** *118*, 154–161, https://doi.org/10.1016/j.saa.2013.08.075.
29. Al-Shamry, A.A.; Khalaf, M.M.; El-Lateef, H.M.A.; Yousef, T.A.; Mohamed, G.G.; El-Deen, K.M.K.; Gouda, M.; Abu-Dief, A.M. Development of New Azomethine Metal Chelates Derived from Isatin: DFT and Pharmaceutical Studies. *Materials* **2023,** *16*, 83. https://doi.org/10.3390/ma16010083.
30. Nagesh, G.Y.; Raj, K.M.; Mruthyunjayaswamy, B.H.M. Synthesis, characterization, thermal study and biological evaluation of Cu(II), Co(II), Ni(II) and Zn(II) complexes of Schiff base ligand containing thiazole moiety. *J. Mol. Struct.* **2015,** *1079*, 423–432, https://doi.org/10.1016/j.molstruc.2014.09.013.
31. Ali, M.A.; Bakar, H.J.H.A.; Mirza, A.H.; Smith, S.J.; Gahan, L.R.; Bernhardt, P.V. Preparation, spectroscopic characterization and X-ray crystal and molecular structures of nickel (II), copper (II) and zinc (II) complexes of the Schiff base formed from isatin and S-methyldithiocarbazate (Hisa-sme). *Polyhedron* **2008,** *27*, 71-79, https://doi.org/10.1016/j.poly.2007.08.022.
32. Naik, K.H.N.K.; Bhimareddy, A., Naik, N. ChemInform Abstract:Ruthenium metal complexes and their biological approach - A short review. *Chem. Inform.* **2015,** *46* , https://doi.org/10.1002/chin.201541240.
33. Raman, N.; Selvan, A.; Sudharsan, S. Metallation of ethylenediamine based Schiff base with biologically active Cu (II), Ni (II) and Zn (II) ions: Synthesis, spectroscopic characterization, electrochemical behaviour, DNA binding, photonuclease activity and *in vitro* anti-microbial efficacy. *Spectrochim. Acta A Mol. Biomol. Spectrosc.* **2011,** *79*, 873-883, https://doi.org/10.1016/j.saa.2011.03.017.
34. Jeon, S.; Moncol, J.; Mazúr, M.; Valko, M.; Choi, J.-H. Synthesis, Crystal Structure, Spectroscopic Properties, and Hirshfeld Surface Analysis of Diaqua [3,14-dimethyl-2,6,13,17 tetraazatricyclo(16.4.0.0^{7,12})docosane]copper(II) Dibromide. *Crystals* **2019,** *9*, 336. https://doi.org/10.3390/cryst9070336.
35. Enamullah, M.; Zaman, M.A.; Bindu, M.M.; Islam, M.K.; Islam, M.A.Experimental and theoretical studies on isatin-Schiff bases and their copper(II)-complexes: Synthesis, spectroscopy, tautomerism, redox potential, EPR, PXRD and DFT/TDDFT. *J. Mol. Struct.* **2020,** *1201*, 127207, https://doi.org/10.1016/j.molstruc.2019.127207.
36. El-Tabl, A.S.; El-Saied, F.A.; Plass, W.; Al-Hakimi, A.N. Synthesis, spectroscopic characterization and biological activity of the metal complexes of the Schiff base derived from phenylaminoacetohydrazide and dibenzoylmethane. *Spectrochim. Acta A Mol. Biomol. Spectrosc.* **2008,** *71*, 90–99, https://doi.org/10.1016/j.saa.2007.11.011.
37. Mahmoud, W.H.; Mohamed, G.G.; El-Sayed, O.Y. Coordination compounds of some transition metal ions with new Schiff base ligand derived from dibenzoyl methane. Structural characterization, thermal behavior, molecular structure, anti-microbial, anticancer activity and molecular docking studies. *Appl. Organomet. Chem.* **2018,** *32*, e4051, https://doi.org/10.1002/aoc.4051.
38. Kaur, M.; Kaushal, R. Synthesis, characterization and α-amylase and α-glucosidase inhibition studies of novel vanadyl chalcone complexes. *Appl. Organomet. Chem.* **2021,** *35*, e6042, https://doi.org/10.1002/aoc.6042.
39. Szklarzewicz, J.; Jurowska, A.; Hodorowicz, M.;Kazek, G.; Mordyl, B.; Menaszek, E.; Sapa, J. Characterization and antidiabetic activity of salicylhydrazone Schiff base vanadium(IV) and (V) complexes. *Transit. Met. Chem*. **2021,** *46*, 201–217 https://doi.org/10.1007/s11243-020-00437-1.
40. Wu, P.; He, H.; Ma, H.; Tu, B.; Li, J.; Guo, S.; Chen, S.; Cao, N.; Zheng, W.; Tang, X.; Li, D.;Xu, X.; Zheng, X.; Sheng, Z.; Hong, W.D.; Zhang, K. Oleanolic acid indole derivatives as novel α-glucosidase inhibitors: Synthesis, biological evaluation, and mechanistic analysis. *Bioorg. Chem.* **2021,** *107*,104580, https://doi.org/10.1016/j.bioorg.2020.104580.
41. Sudha, A.; Askar ali, S.J. Investigation of new schiff base transition metal (II) complexes theoretical, antidiabetic and molecular docking studies. *J. Mol. Struct.* **2022,** *1259*, 132700, https://doi.org/10.1016/j.molstruc.2022.132700.
42. Anu, D.; Naveen, P.; Rath, N.P.; Kaveri, M.V. Palladium (II) complexes containing substituted thiosemicarbazones. Synthesis, spectral characterization, X-ray crystallography, biomolecular interactions and *invitro* cytotoxicity. *J. Mol. Struct.* **2020,** *1206*, 127703, https://doi.org/10.1016/j.molstruc.2020.127703.
43. Wassel, M.M.S.; Ragab, A.; Ali, G.A.M.E.; Mehany, A.B.M.; Ammar, Y.A. Novel adamantane-pyrazole and hydrazone hybridized: Design, synthesis, cytotoxic evaluation, SAR study and molecular docking simulation as carbonic anhydrase inhibitors. *J. Mol. Struct.* **2021,** *1223*,128966, https://doi.org/10.1016/j.molstruc.2020.128966.

Supplementary materials

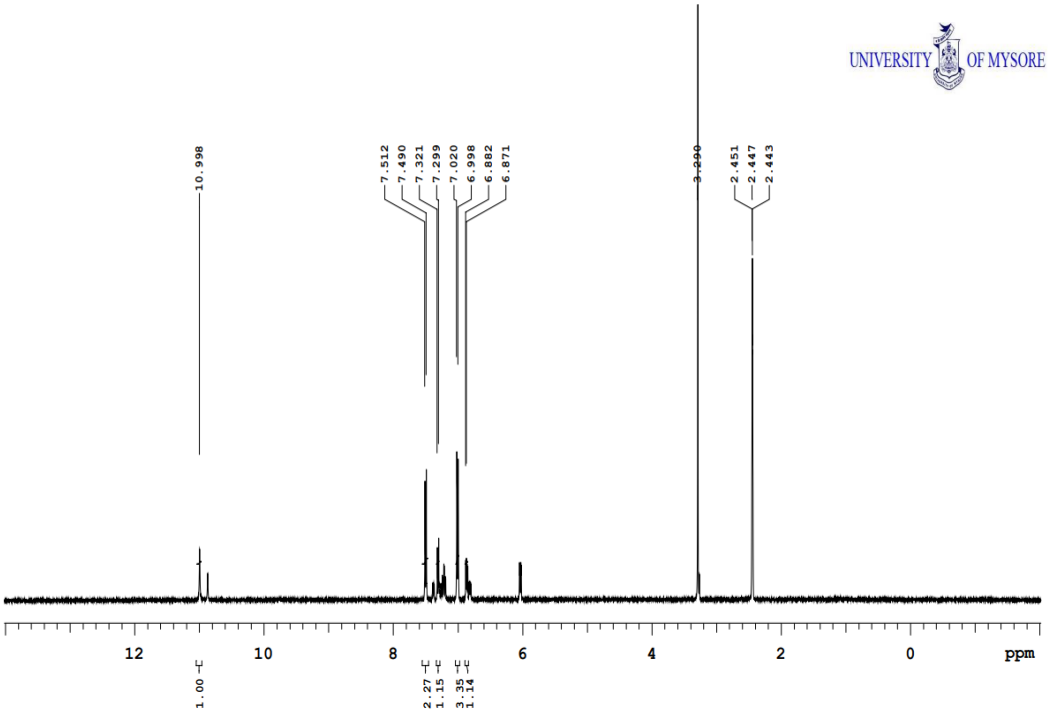

Figure S1. ^{1}H NMR of ligand **(L6).**

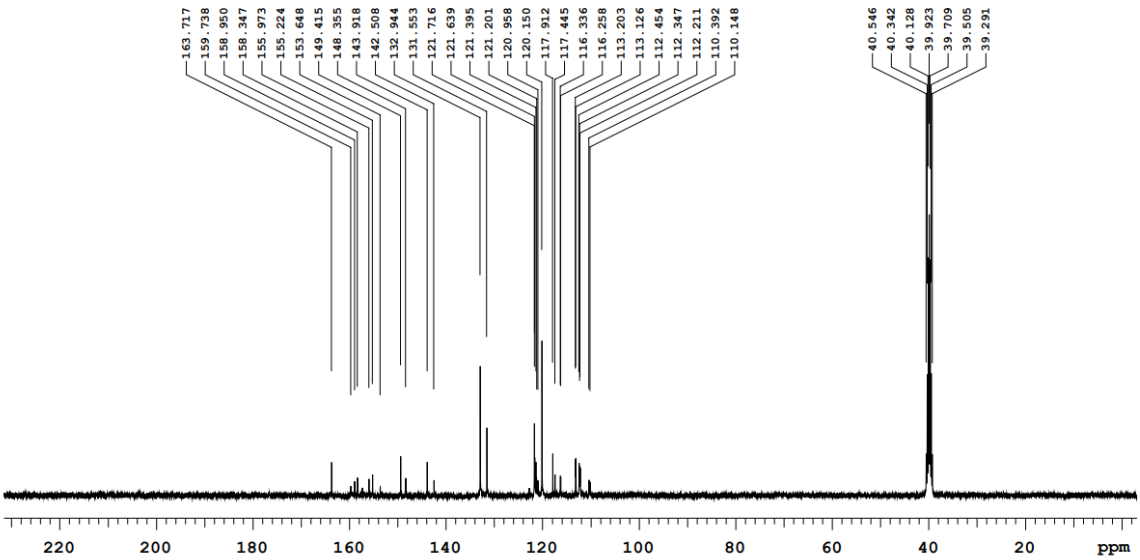

Figure S2. ^{13}C NMR of ligand **(L6).**

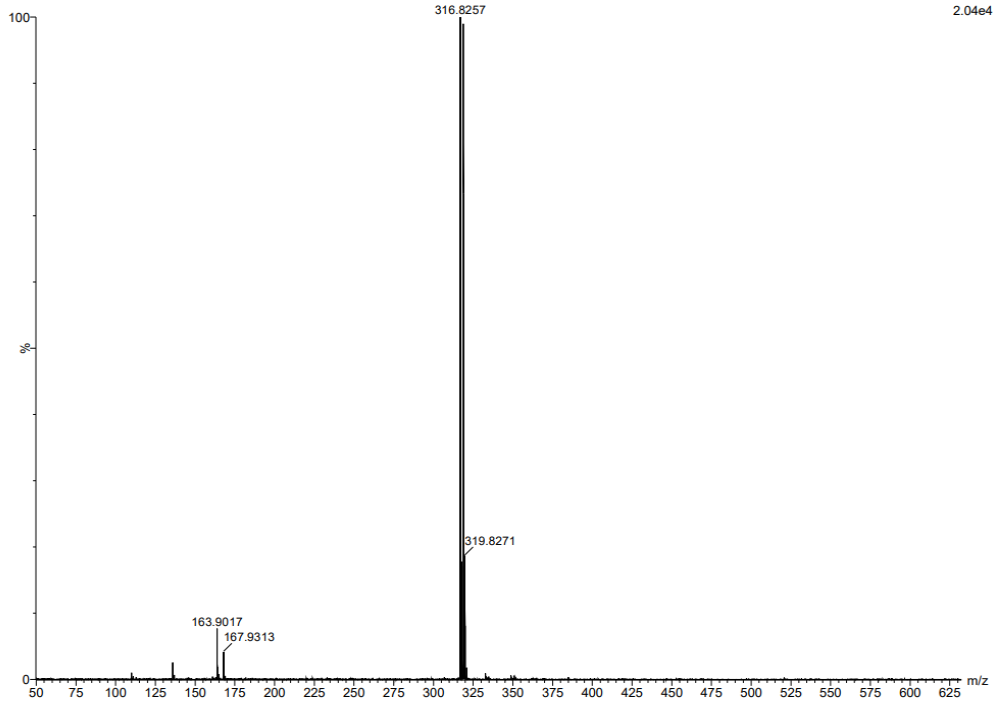

Figure S3. Mass Spectrum of Ligand **(L6).**

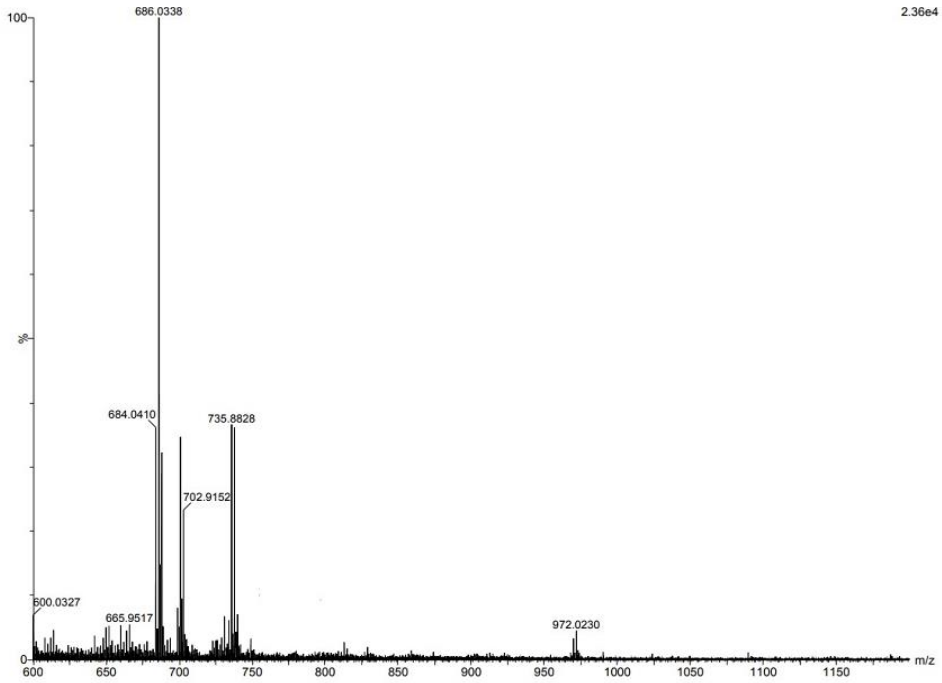

Figure S4. Mass Spectrum of **(6a).**

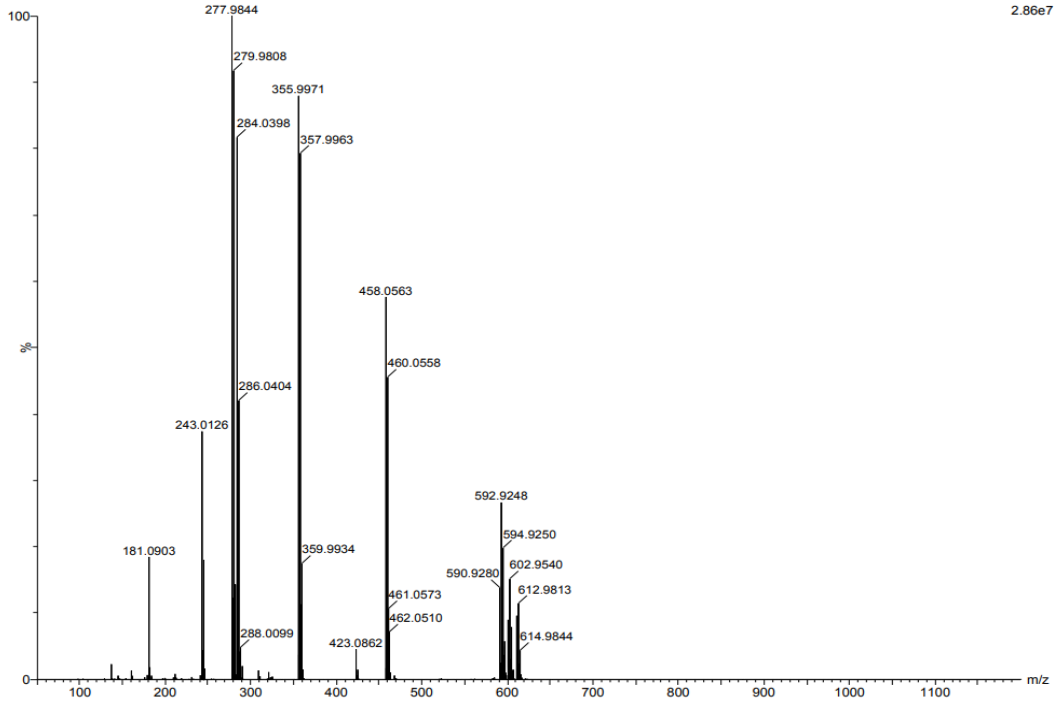

Figure S5. Mass Spectrum of **(6b).**

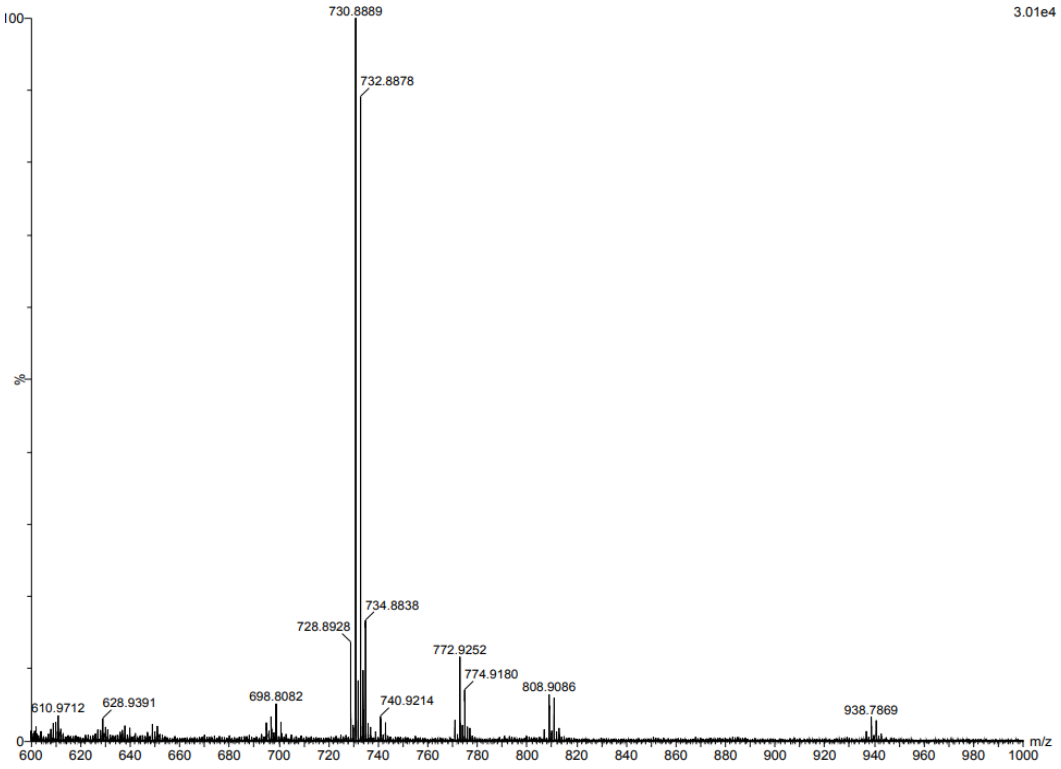

Figure S6. Mass Spectrum of **(6c).**

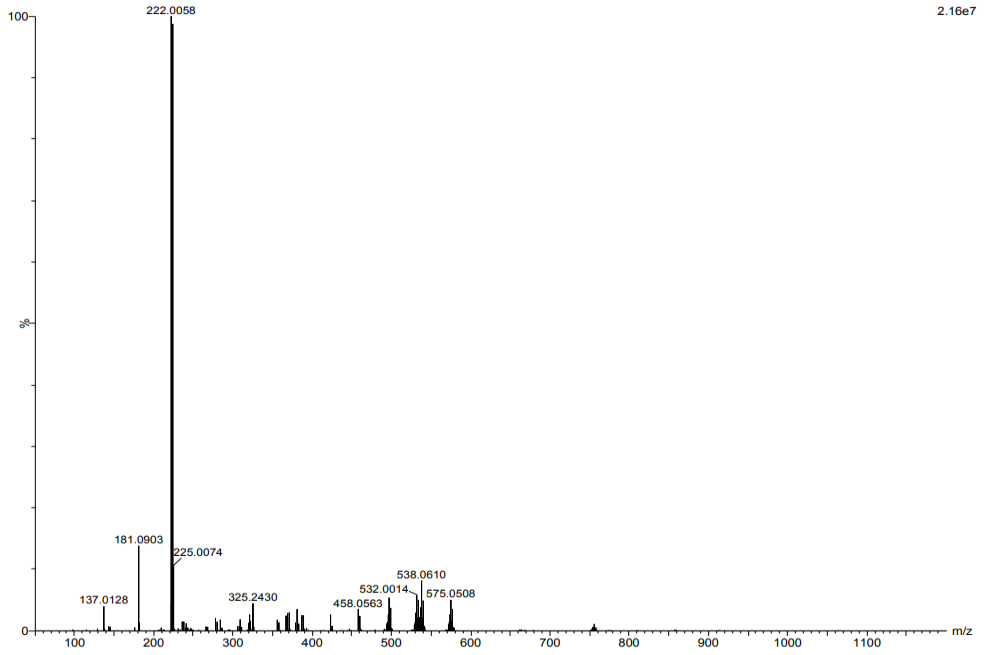

Figure S7. Mass Spectrum of **(6d).**

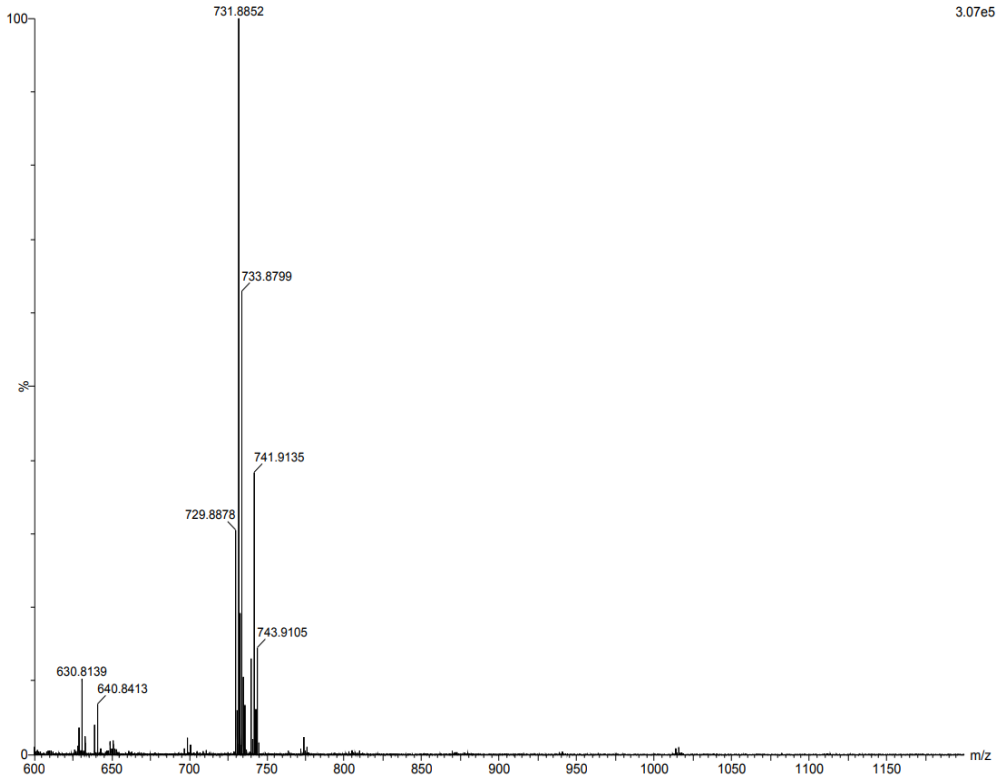

Figure S8. Mass Spectrum of **(6e).**

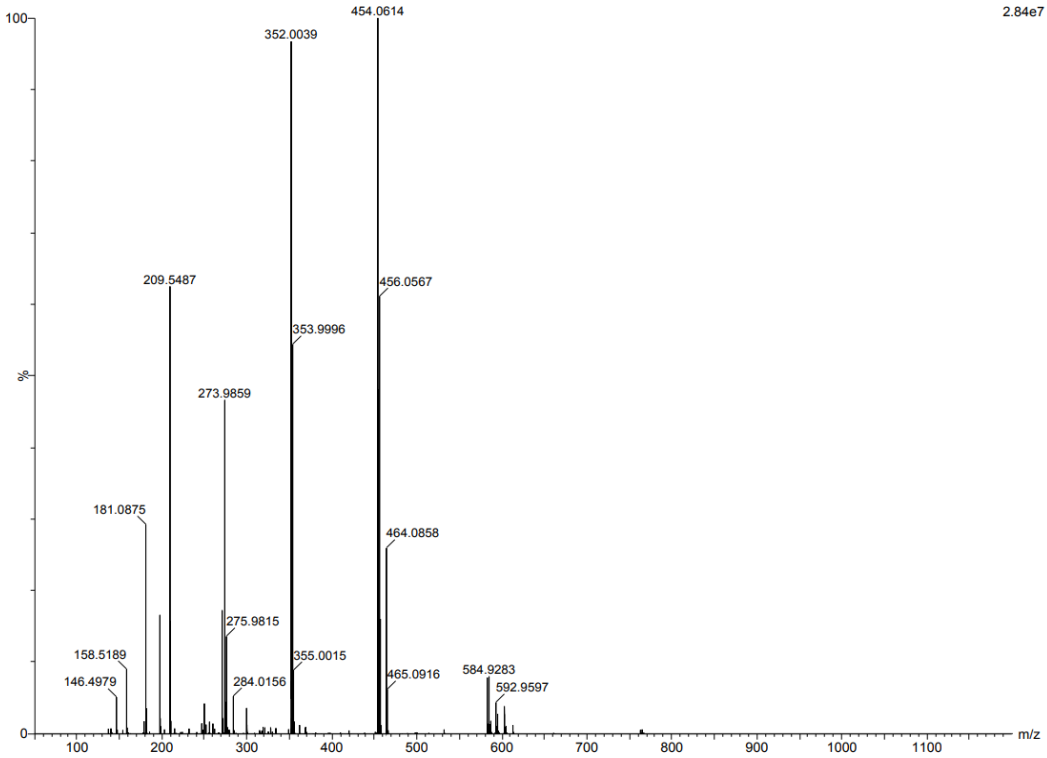

Figure S9. Mass Spectrum of **(6f).**

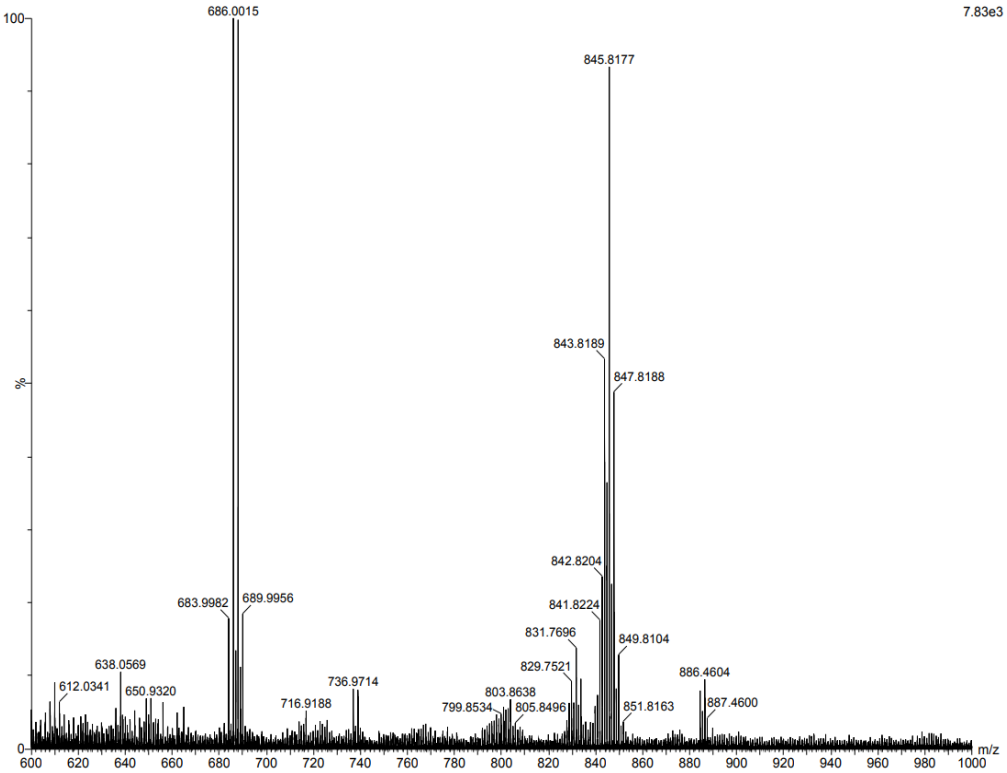

Figure S10. Mass Spectrum of **(6g).**

Figure S11. Mass Spectrum of **(6h).**